5101-137
Low-Cost
Solar Array Project



DOE/JPL-1012-32
Distribution Category UC-63b

# Fracture Strength of Silicon Solar Cells

C.P. Chen

October 15, 1979

Prepared for
U S. Department of Energy
Through an agreement with
National Aeronautics and Space Administration
by
Jet Propulsion Laboratory
California Institute of Technology
Pasadena, California

(JPL PUBLICATION 79-102)

5101-137
Low-Cost
Solar Array Project

DOE/JPL-1012-32
Distribution Category UC-63b

# Fracture Strength of Silicon Solar Cells

C.P. Chen



October 15, 1979

Prepared for
U.S. Department of Energy
Through an agreement with
National Aeronautics and Space Administration
by
Jet Propulsion Laboratory
California Institute of Technology
Pasadena, California

(JPL PUBLICATION 79-102)

REA

Prepared by the Jet Propulsion Laboratory, California Institute of Technology, for the Department of Energy through an agreement with the National Aeronautics and Space Administration.

The JPL Low-Cost Solar Array Project is sponsored by the Department of Energy (DOE) and forms part of the Solar Photovoltaic Conversion Program to initiate a major effort toward the development of low-cost solar arrays.

## ACKNOWLEDGMENT

The author gratefully acknowledges the assistance and encouragement of many members of the Engineering Area of the Low-cost Solar Array (LSA) Project, particularly that of Dr. Ron Ross, Mr. Jim Arnett, and Mr. Ed Royal. Special thanks are extended to Dr. Marty Leipold of the Materials Research and Technology Group at JPL for his continuing guidance and contributions to this study.

## ABSTRACT

In an effort to improve the reliability and lower the cost of solar cells, a test program has been developed to determine the nature and source of the flaw controlling the fracture of silicon solar cells and to provide information regarding the mechanical strength of cells.

This report contains results obtained in the first phase of a test program to develop improved methods for testing the mechanical strength of cells and to evaluate the fracture strength of typical Czochralski silicon solar cells 76 mm (3 in.) in diameter.

Significant changes in fracture strengths were found in seven selected in-process wafer-to-cell products from a manufacturer's production line. The fracture strength data were described by Weibull statistical analysis and can be interpreted in light of the exterior flaw distribution of the samples.

CONTENTS

Figures

Tables

## SECTION I

## SUMMARY

This report presents the results of an in-house test program at JPL for the Engineering Area of the DOE/JPL Low-cost Solar Array (LSA) Project by the Materials Research and Technology Group, Applied Mechanics Division of the Jet Propulsion Laboratory, California Institute of Technology. The objective of this test program was to evaluate cell cracking characteristics and fracture strength changes in the in-process wafer-to-cell end items taken at different stages of a typical manufacturer's production line. It is anticipated that the information on the nature and source of flaws controlling the fracture of silicon solar cells can lead to enhanced production yields and thus to lower costs.

This effort involved the design, evaluation and assessment of several mechanical strength test methods, and study of their limitations for testing silicon solar cells. A specially designed four-point twisting test was recommended as a standard method or measurement of the mechanical strength of silicon solar cells because of its advantageous characteristics over other conventional methods.

The study was made on typical 3-inch diameter Czochralski silicon wafers and cell samples at seven selected stages in the production cycle of a manufacturer. The test results are summarized in Table 1-1. Significant changes in fracture strength were found as a result of the cell processing steps. The strength of chemically polished wafers increased to more than twice that of as-cut wafers; however, the chemical polishing was not sufficient to reduce the large flaws in the samples, suggesting that more chemical polishing is necessary. A significant increase in the overall strength of wafers from texture etching was evident when texture etched wafers were compared with as-sawn wafers. The strength of completed cells varied with the lot number.

The results of this test program indicate that the strength of silicon wafers and cells is controlled by preexisting exterior (edge and surface) flaws which were generated during wafering or handling. The large critical flaws occurring during a cell process step are carried on to the subsequent processes. The fracture strength data were described by Weibull statistical analysis and can be interpreted in light of the exterior flaw distribution of the samples.

A long tail at the low stress portion of the strength distribution curve was found for several types of samples. The wafers or cells, which in the low strength distribution contain large flaws, are likely to be fractured during subsequent cell processing and handling or in the field service. A proof test would be desirable to eliminate these samples before the subsequent cracking occurs.

**Table 1-1. Summary of Test Results**

CYLINDRICAL BENDING

| Sample Type | Orientation | Strength ($MNm^{-2}$) | | Mean Deflection at Failure (mm) |
|---|---|---|---|---|
| | | 50% Failure Probability | Range of 90% of Failure | |
| As-cut Wafer | <100> | 134 | 110-138 | 1.4 |
| As-cut Wafer | <110> | 117 | 112-132 | 1.3 |
| Chem. Polished Wafer | <110> | 278 | 132-336 | 2.8 |
| Chem. Polished Wafer | 22.5° off <110> | 289 | 136-363 | 3.0 |

BIAXIAL STRENGTH

| Sample Type | Strength ($MNm^{-2}$) | | Mean Deflection at Failure (mm) |
|---|---|---|---|
| | 50% Failure Probability | Range of 90% of Failure | |
| As-cut wafer | 194 | 165-246 | 1.3 |
| Chem. Polished Wafer | 496 | 186-841 | 3.3 |
| Texture Etched Wafer | 379 | 248-455 | 2.3 |

**Table 1-1. Summary of Test Results (Continued)**

FOUR-POINT TWISTING

| Sample Type | Strength ($MNm^{-2}$) | | Mean Deflection at Failure (mm) |
|---|---|---|---|
| | 50% Failure Probability | Range of 90% of Failure | |
| ...e-cut Wafer | 93 | 45-103 | 2.0 |
| Chem. Polished Wafer | 217 | 83-386 | 4.8 |
| Edge Rounded Wafer | 92 | 58-110 | 2.5 |
| Texture Etched Wafer Lot B | 162 | 151-186 | 2.5 |
| Texture Etched Wafer Lot E | 176 | 60-190 | 3.5 |
| Texture Etched Wafer Lot F | 208 | 144-229 | 3.6 |
| Mesa Etched and A/R Coated Wafer | 214 | 110-293 | 3.9 |
| Pre-Ohmic Cell Lot A | 172 | 31-248 | 2.9 |
| Completed Cell Lot A | 152 | 55-234 | 3.3 |
| Completed Cell Lot C | 207 | 103-262 | 3.6 |
| Completed Cell Lot E | 214 | 131-296 | 3.4 |

## SECTION II

## INTRODUCTION

The cracking cell is one of the major sources of solar panel rejection and failure (References 1, 2). Cracking of silicon solar cells during field service and testing is believed to result from the extension of a critical preexisting flaw under stress. Such flaws, probably generated during silicon wafering and cell processing and handling, may therefore control the mechanical strength of silicon solar cells. This information emphasizes the importance of establishing a standard mechanical testing method for evaluating the mechanical strength of silicon solar cells. The data resulting from such testing could be used by manufacturers of solar cells to enhance production yields, improve cell reliability and durability, and ultimately to establish mechanical design criteria that would reduce cell cost and support development of automated production.

A silicon solar cell is an ultrathin disc. Because of various limitations inherent in this unique configuration, standard mechanical testing methods are not readily applicable to stressing a large area of the cell specimen uniformly.

A program for mechanical testing of silicon cells was implemented at JPL in July 1978. The purpose of this report is to present the results obtained from the first phase of this test program, which included the following tasks:

(1) Identification of important factors affecting the strength of silicon solar cells

(2) Determination of a test method to measure cell strength

(3) Design and fabrication of a test jig

(4) Procurement of cell samples

(5) Preliminary test and jig modification

(6) Generation of data regarding typical solar cells

(7) Analysis of test data.

Strength data resulting from studies of brittle materials typically show a great deal of scatter. For this reason the conventional method of representing observed quantities using the arithmetic mean and its standard deviation may not show a meaningful characteristic of strength distribution. A statistical method commonly used to describe the strength of brittle materials is that given by Weibull (References 3, 4). According to this method, a

formula of the form given below is used to relate the probability of failure, G, with stress, S.

$$G = 1 - \exp\left[-\int_V \left(\frac{S - S_u}{S_o}\right)^m dV\right] \qquad (1)$$

where $S_u$ is the stress below which none of the samples will fail, $S_o$ is a normalizing factor, m is termed the Weibull modulus, and V is the volume of material under uniaxial stress where fracture initiates. $S_u$, $S_o$ and m are material properties and are called Weibull parameters. In Weibull analysis it is assumed that fracture at the most critical flaw under a given stress distribution leads to total failure. Thus, the Weibull method is also called "Weakest Link Statistics".

For material under bending, the critical flaw which causes fracture is mostly on the surface. Thus, the fracture probability, G, for material under bending can be expressed as function of surface area, A:

$$G = 1 - \exp\left[-\int_A \left(\frac{S - S_u}{S_o}\right)^m dA\right] \qquad (2)$$

From this equation it is apparent that the larger the surface area of the material under bending stress, the lower the strength distribution obtained from the test. This phenomenon can be interpreted to mean that the larger the surface area under stress, the greater the probability of finding a larger flaw. Therefore, strength data of brittle material depends on both the test sample size and the test method in which the surface area of the sample is stressed.

The typical Weibull plot to describe strength data of brittle material is shown in Figure 2-1. The strength distribution of this Weibull plot can also be described by the distribution of the critical flaw size in the samples. The larger flaw size is found in the fractured sample at the left-hand side (lower strength) of the curve, while the smaller flaw size is at the right-hand side of the curve.

It is important to note that the Weibull modulus, m, which describes the slope of the curve, is related to the flaw size distribution of a material. The smaller m value indicates greater distribution of flaws, greater scatter of the strength data, and shows a smaller slope on the Weibull curve. The Weibull plot will be used to display and interpret the general characteristics of strength data on silicon solar cells.

A brief assessment of several mechanical strength test methods that are most feasible for testing silicon solar cells is given in Section III of this report, and their limitations are addressed. From

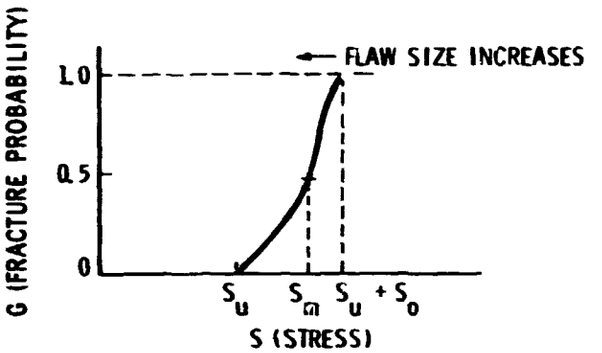


FRACTURE PROBABILITY $G = 1 - \exp\left[-\int_V \left(\frac{S - S_u}{S_o}\right)^m dV\right]$

$S_u$ = STRESS BELOW WHICH NONE WILL FAIL

$S_u + S_o$ = STRESS ABOVE WHICH ALL WILL FAIL

$S$ = STRESS OF INTEREST

$m$ = WEIBULL MODULUS (RELATE TO SLOPE OF PLOT)

$S_m$ = S AT 0.5 G, $S_m \approx S_{ave}$

Figure 2-1. Typical Weibull Distribution (Weakest Link Statistics) of Strength Data of Brittle Material

this discussion, a standard method for testing solar cell samples is recommended. Section IV describes the solar cell testing program, which includes specimen selection, apparatus design and measured results. A discussion of test results in terms of loading conditions and the nature of cell processing steps by using Weibull statistical analysis is presented in Section V. Major conclusions resulting from the conduct of this test are presented in Section VI. Recommendations for future work are given in Section VII. Equations for stress calculation of the test configurations are presented in Appendix A. Detailed measured cell strength data is given in Appendix B.

## SECTION III

## TEST METHOD ASSESSMENT

### A. OBJECTIVE

Conventional methods for testing the strength of ceramic materials are not readily applicable to a thin circular disk like a silicon solar cell because of various limitations inherent in the cell itself. First of all, the thickness to span or width ratio is too small to meet the requirements for conventional test method specimens. Moreover, using conventional methods, stress is concentrated at loading points, producing large deflection, and only a limited portion or none of the cell edge is stressed. Edge flaws are most frequently the origin of fractures in cracked cells. Stress distribution is further complicated by the circular shape of the silicon cell, which imposes additional boundary conditions.

For meaningful interpretation of fracture strength data of silicon solar cells Weibull statistical analysis must be used. Weibull analysis assumes that fracture of brittle material at the most critical flaw under a given stress leads to total failure. The larger the surface area of material under stress, the greater the probability of finding a larger flaw, and the lower the strength distribution that is obtained from the test.

A number of test configurations and loading systems were examined in this study for possible use in determining the strength of silicon solar cells. Detailed analyses were carried out, with emphasis on the following criteria:

(1) Simple configuration

(2) Easy to perform

(3) Easy to adapt in a cell production line

(4) Self aligning

(5) Able to stress a large area uniformly.

The "conventional" test methods determined to be most feasible for this purpose were the cylindrical bending test and the biaxial flexure strength test. A specially designed test method referred to as "four-point twisting" had not been evaluated previously but was examined in detail in this study. This test is shown to have desirable features which make it particularly useful for testing the strength of thin disk samples such as silicon solar cells.

## B. ANALYSIS OF TESTS

### 1. Cylindrical Bending Test

This method is used conventionally to determine the modulus of rupture (MOR) strength of material for bar or plate samples. The loading method is shown schematically in Figure 3-1. The calculation of MOR strength of material is given in Appendix A.

According to ASTM standards (Reference 5) the thickness to span and width ratio of the specimen for the MOR test should be greater than 1/10 or the following factors should be considered:

(1) Stress concentration at the loading point

(2) Large deflection

(3) Biaxial stress in the center area of the specimen.

The effect of these factors on the measured MOR value were discussed by Giovan (Reference 6). A quantitative evaluation of these factors on the MOR values of silicon solar cells is beyond the scope of present report. However, a strain gage evaluation of a dummy cell under this loading system indicated that the effect of biaxial stress in the center area of a specimen on the MOR value of a solar cell is negligible.

Since the cross-sectional area of the circular specimen under cylindrical bending varies, the stress distribution curve shown in Figure 3-1 deviates from a straight line. In other words, the maximum stress inside is not constant, and the stress distribution would curve concavely downward. The amount of deviation from a straight line depends upon the difference between D and D' in Figure 3-1.

To evaluate the extent of the non-uniformity of stress distribution, a finite element computer analysis of a 3-inch diameter circular disc under cylindrical bending was carried out. The result shows that the maximum stress non-uniformity is less than 10%. Therefore, under the cylindrical bending test the stress distribution of a silicon solar cell can be assumed to be constant, as shown in Figure 3-1, and the MOR value can be estimated by Equation A-2 of Appendix A.

Since the bending stress at the extreme fibers of the sample under cylindrical bending is uniaxial, this test would be useful to determine the uniaxial tensile strength of silicon wafers at different crystalline orientations. The effect of crystalline orientation on the MOR strength of silicon wafers will be discussed later.

One drawback of this test is that only portions of the sample and edges of the sample are stressed. Due to the stress concentration under the loading points, the inner span of the test fixture must be designed in such a way that less than 25% of the wafer edge is tested. This limitation has made this test less desirable for evaluation of the mechanical strength of silicon solar cells.

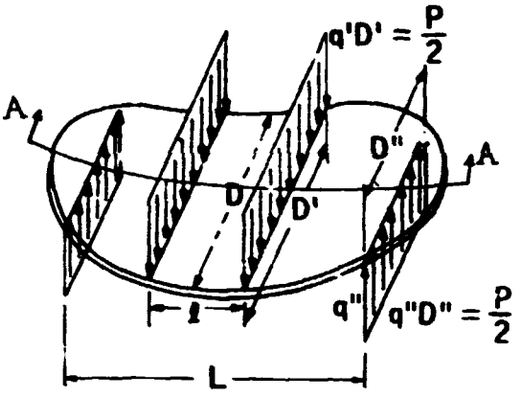


SCHEMATIC

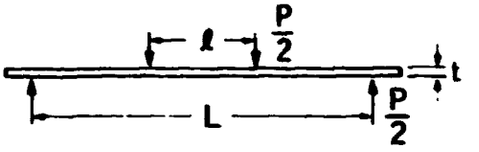


SIDE VIEW OF A-A SECTION


STRESS DISTRIBUTION OF A-A

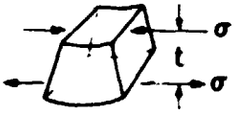


UNIT WIDTH ELEMENT WITHIN ℓ AREA

Figure 3-1. Cylindrical Bending of a Solar Cell

2. Biaxial Flexure Strength Test

This test method is used to evaluate the effect of biaxial stress on the strength of a silicon cell. It is described in ASTM F394-74T (Reference 7) for the determination of biaxial flexure strength of thin ceramic substrates. The loading method is shown schematically in Figure 3-2. The stress calculation is given in Appendix A.

This test method has been studied rather extensively on glass (Reference 8) and ceramics (References 6, 9). The details of stress distributions were described (Reference 10). The conditions of use of this test are given as follows (see Figure 3-2):

(1) The thickness of the plate should not be greater than 1/5 of the diameter of the support ($t \leq 0.4\ a$).

(2) The maximum deflection ($\delta_f$) should be less than half the thickness ($\delta_f \leq 0.5\ t$).

(3) The radius of the center loading plunger should be greater than or equal to 1.7 times of the thickness ($b \geq 1.7\ t$)

In order to determine the strength of silicon solar cells, the test method should be able to stress sample areas as large as possible. Since the thickness (t) of the solar cell is so small, the use of the biaxial strength test for solar cells cannot meet condition 2 and can cause stress concentration at the center loading ring. In addition, the maximum stressed surface area in this test is confined within the central region of the specimen; fracture is not dependent upon the condition of the specimen's edge which has been found to be the major source of cell cracking.

Despite these disadvantages and limitations, this test method is simple and symmetrical, and appears to be useful to determine the relative intrinsic strength of the solar cell. Above all, data regarding the biaxial strength of silicon is of interest and importance for engineering purposes.

In order to minimize stress concentration, the biaxial strength test jig should be designed in such a manner that the central equibiaxial stress area is small, e.g., limited to 12.7 mm (0.5 in.) in diameter. Therefore, a very small central region (~10% of total area) was tested by this test. The biaxial stress can be calculated by Equation A-3 in Appendix A. The stress distribution was verified by the strain gage measurement.

3. Four-Point Twisting Test

This method is used to evaluate the twist (shear) strength of a silicon cell. The cell sample is loaded by four equal vertical forces that are equally spaced at the edge: two diagonally opposite forces acting upwards and the other two acting downwards, as shown

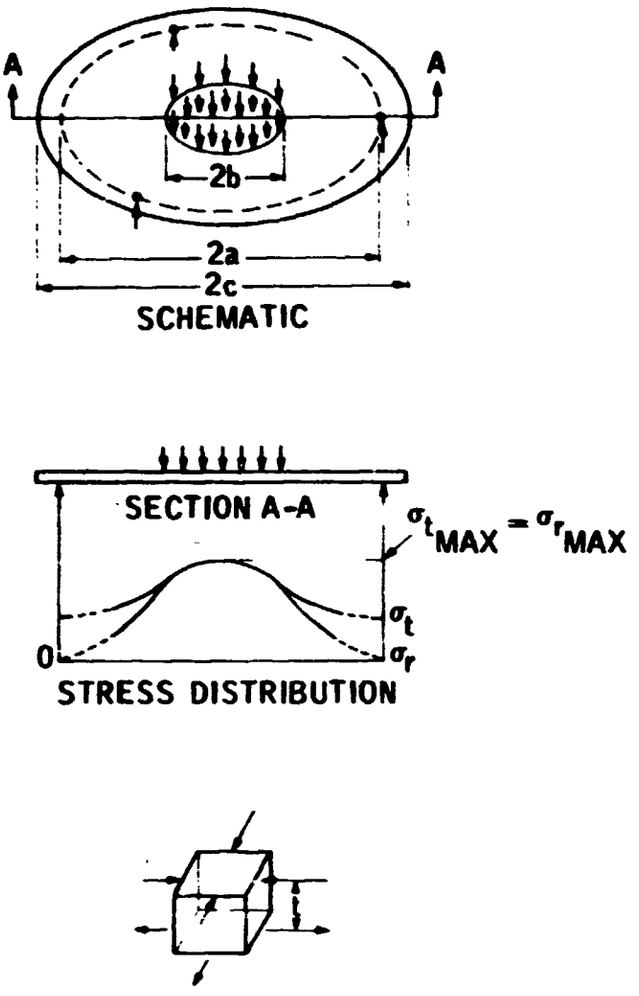


Figure 3-2. Biaxial Strength Test of a Solar Cell

schematically in Figure 3-3. The shear stress calculation is given in Appendix A.

A finite element computer analysis of a 76 mm (3 in.) diameter elastic disc subjected to four-point twisting was carried out; a stress concentration was found at the area of loading points. This problem may make the stress distribution complicated in this area. However, in the area away from the loading points, a uniform shear stress is found in the direction 45° from the axes of two pairs of loading (Figure 3-3). This stress distribution has been verified essentially by strain gage examination.

A stress analysis of a rectangular cross section member subjected to a torsion, T, was made (Reference 11). The maximum twist

stress $\tau_s$ for a circular disc under four-point twisting is derived in Appendix A and can be estimated by Equation A-6.

$$\tau_s = \frac{3P}{2t^2}$$

where t is the thickness of the wafer

P is the total fracture force

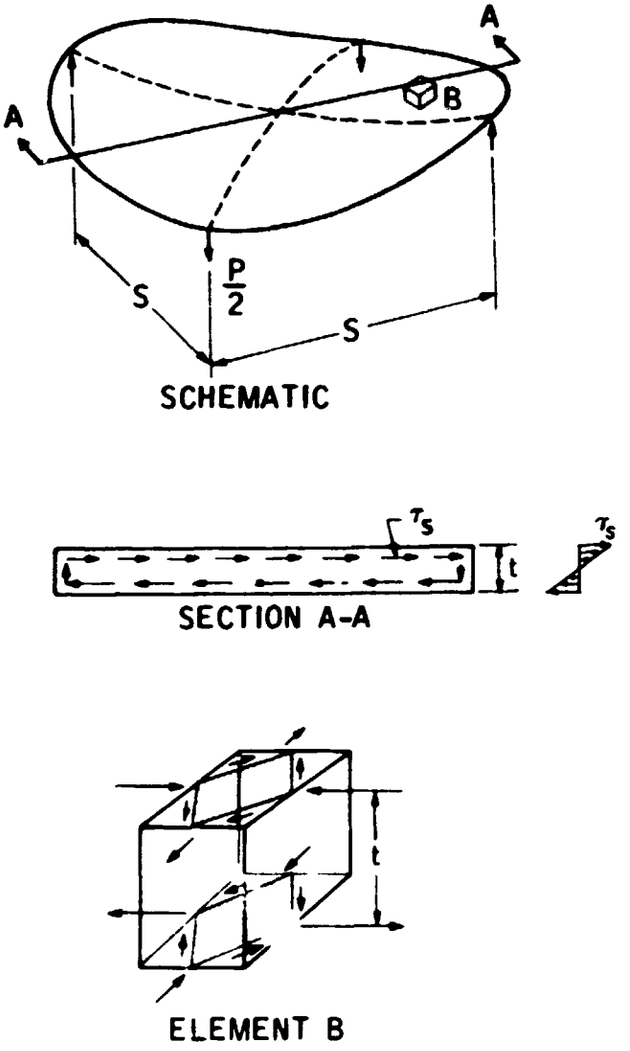


Figure 3-3. Four-point Testing of a Solar Cell

The expected limitations of this test method, such as stress concentrations and large deflection, are beyond the scope of the present report and have not been examined. It is recommended that these areas be investigated in more detail analytically and experimentally.

The four-point twisting test has a simple loading configuration, self alignment, is symmetrical, easy to perform, and stresses the entire wafer specimen, including the edge and internal areas.

## C. CONCLUSIONS

The limitations that are common to all three test methods, i.e., stress concentrations at the load point and large deflection, appear to be due to the form of the solar cell sample itself. These limitations can be minimized by proper test jig design, such as use of a teflon washer at the loading point.

Cylindrical bending proved to be useful to determine the uniaxial tensile (MOR) strength of silicon wafers at different crystalline orientations. One drawback is that less than 25% of the sample and the sample edges are tested.

The biaxial strength test is simple and symmetrical, and appears to be useful to determine the relative strength of the solar cell. However, this method tests a very small central region of the sample; edges of the sample are not stressed. Edge flaws have been found to be the major source of cell cracking, controlling the fracture strength.

The four-point twisting test not only has a simple and symmetrical loading configuration, but also has self-alignment and is easy to perform. In addition, it stresses the entire wafer specimen, including edges and internal area. Four-point twisting is therefore recommended as a standard method for testing the mechanical strength of silicon solar cells.

## SECTION IV

## SOLAR CELL TESTING

### A. OBJECTIVE

To evaluate cell cracking characteristics and changes in fracture strength of silicon solar cells in a typical production line, a representative manufacturer with processing facilities for the complete end-to-end production of typical 76 mm (3 in.) diameter Czochralski solar cells was identified, and samples were procured and studied at several key cell production process steps. A loading fixture was designed and fabricated to perform mechanical strength tests. The test specimens, test apparatus and test results are described in the following pages.

### B. SPECIMEN

Typical solar cells produced by several manufacturers were considered for use in this test effort. Those selected for study were the products of a specific manufacturer* with processing facilities for the complete end-to-end production of solar cells. Starting from silane and continuing through polycrystalline silicon to single crystal ingots and sawing of wafers, all of the process steps required to make the completed cell are included. In addition, this manufacturer indicated willingness to provide test samples.

The test specimens included a series of wafer and cell samples 76 mm (3 in.) in diameter taken at several process steps** as follows:

(1) As cut wafers (multi-wire slurry wafering)

(2) Chemically polished wafers***

(3) Edge rounded wafers

(4) Texture etched wafers

(5) Mesa etched and anti-reflection (A/R) coated wafers

(6) Pre-ohmic cells

(7) Completed (metallized) cells

---

* Motorola Inc., Semiconductor Division, Phoenix, AZ.

** Processing procedures are proprietary information.

***Chemical polishing is not used in the regular cell processing. These wafer specimens were made from as-cut wafers (no edge rounding) for the strength evaluation only. All other wafers and cells of the subsequent processes were made from edge rounded wafers.

The properties of the silicon material are given as follows: <100> orientation; boron doped, P-type; resistivity ranging from 0.5 to 2.0 ohm-cm.

## C. TEST APPARATUS

A test fixture was designed so that it could perform cylindrical bending tests, three-point support biaxial flexure strength determinations and four-point twisting tests of silicon solar cell by simply rearranging, removing, or adding dowel pins (8 mm in diameter) and components. The fixture arrangement for each test is described below.

### 1. Cylindrical Bending

The cylindrical bending test fixture for solar cells is shown in Figure 4-1. Two lower blocks provide line supports for the cell specimen. Each supporting block is guided into position by three dowel pins and can be pivoted at the middle pin. The upper loading piece was fabricated to be pivoted at a ball bearing at the center. Vinyl electrical tape* was applied on the loading lines of the test fixture to minimize the possibility of stress concentration. The inner span ($\ell$) and outer span (L) (see Figure 3-1) are 25.4 mm (1.0 in.) and 55 mm (2.165 in.), respectively.

### 2. Biaxial Flexure Strength

The biaxial flexure strength test jig for solar cells is shown in Figure 4-2. The specimen is supported by three dowel pins equally spaced in a circle 63.5 mm in diameter. A teflon washer (12.7 mm o.d., 1.7 mm thick) was applied at each contact point of the dowel pin to minimize the stress concentration. The center loading area is also 12.7 mm (0.5 in.) in diameter, the size of the teflon washer at the contact point of the dowel pin. This test fixture was designed for cells 76 mm (3.0 in.) in diameter, which is a typical size for most solar cells currently manufactured. Therefore (see Figure 3-2), 2a = 63.5 mm (2.5 in.), 2b = 12.7 mm (0.5 in.), and 2c = 76.2 mm (3.0 in.).

### 3. Four-Point Twisting

The four-point twist jig for solar cells is shown in Figure 4-3. During the test, two dowel pins on the bottom disk act upwards while the other two, which are 90° apart on the upper disk act downwards to give a shear stress at 45° in the cell specimen, as shown in Figure 3-3. A teflon washer (12.7 mm o.d., 1.7 mm thick) was used at the contact point of each dowel pin. These four dowel pins were designed in a 63.5 mm (2.5 in.) diameter circle.

*Scotch Brand, 33+, 20 mm wide x 0.18 mm thick.

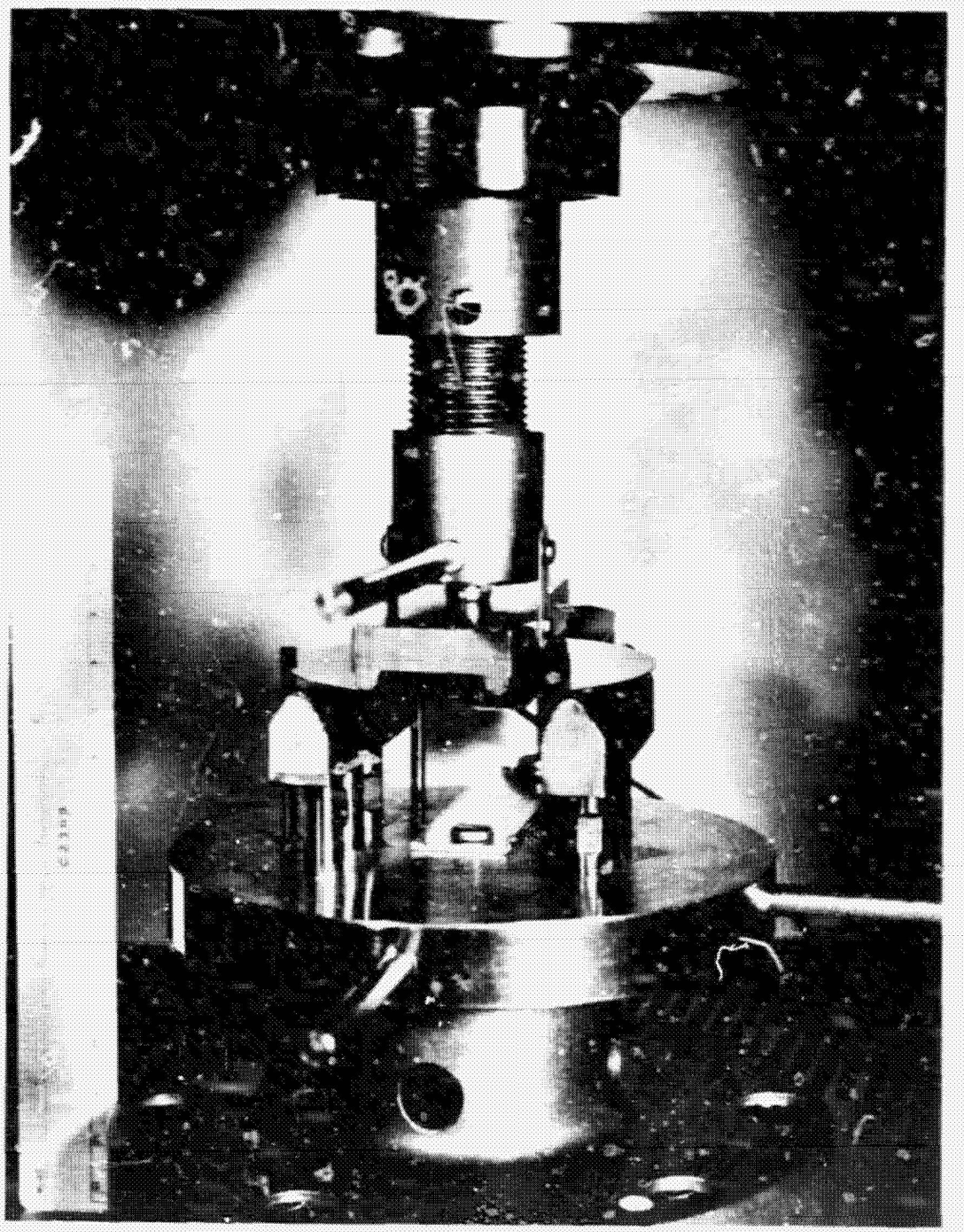

Figure 4-1. Solar Cell Cylindrical Bending Jig

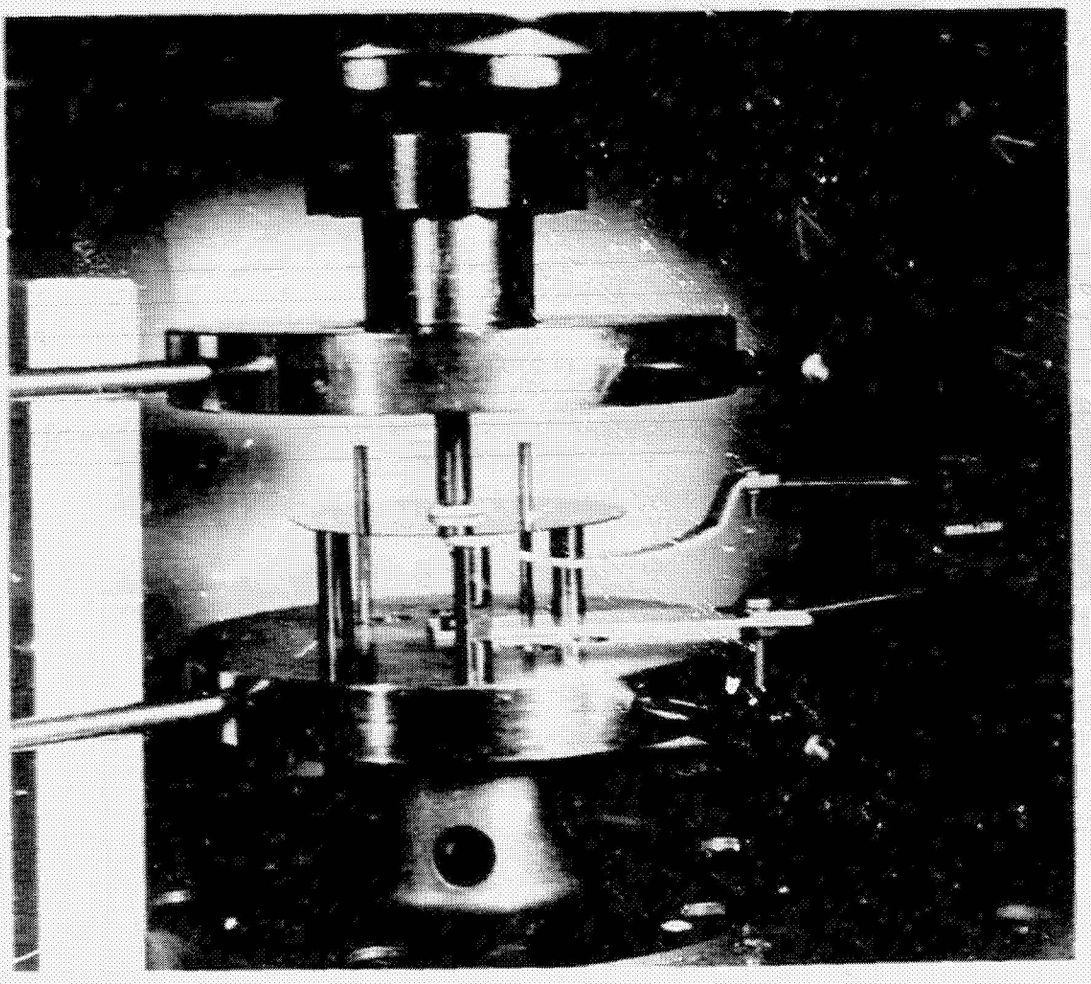

Figure 4-2. Solar Cell Biaxial Flexure Strength Test Jig

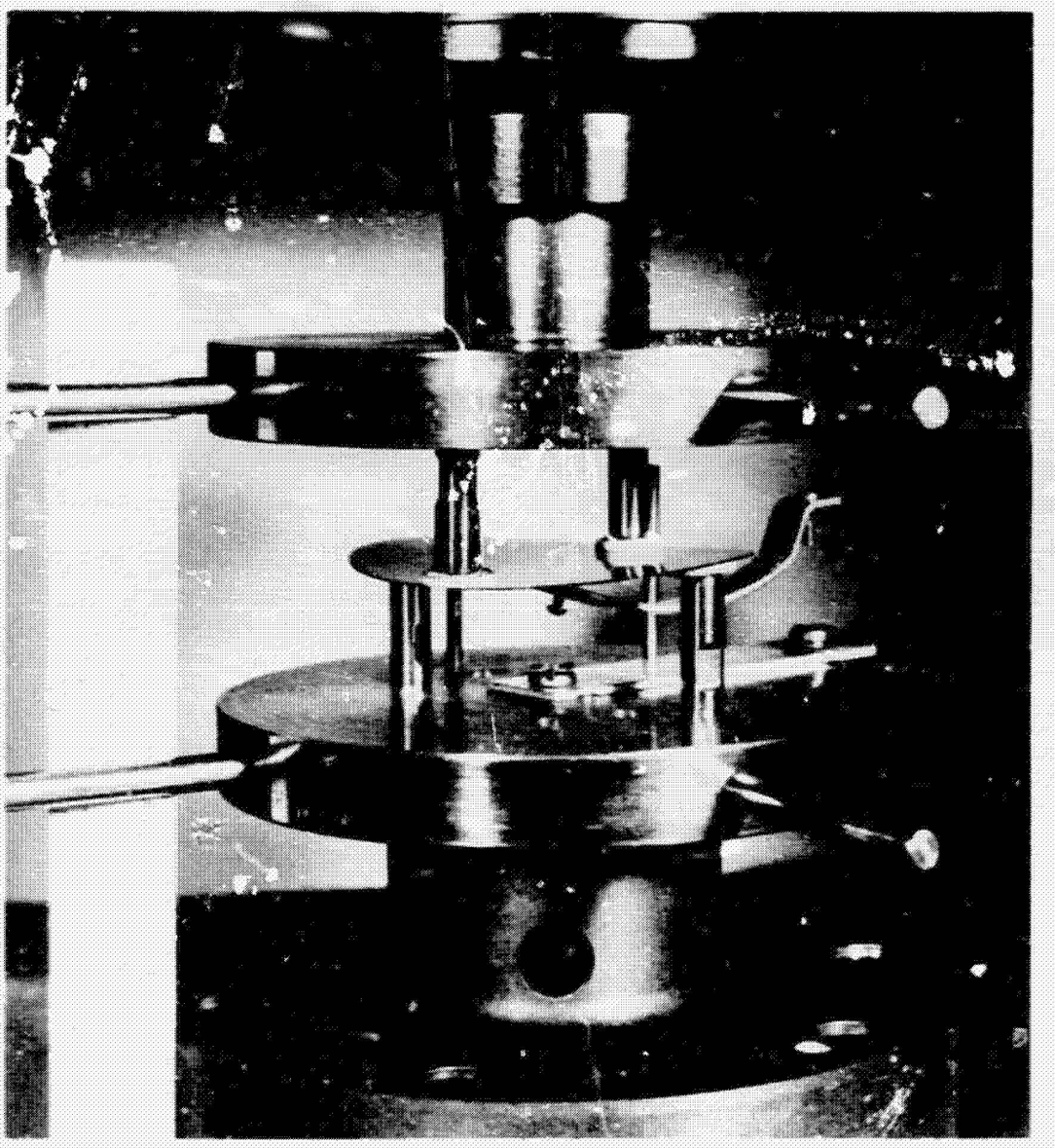

Figure 4-3. Solar Cell Four-point Twist Jig

## D. TEST IMPLEMENTATION

Prior to each test the thickness of each specimen was measured at five positions, as shown in Figure 4-4, in order to determine the thickness variation of the specimen. The maximum thickness variation of wafers was approximately 0.013 mm (~ 0.0005 in.) and that of completed cells was up to 0.05 mm (~ 0.002 in.) because of nonuniform solder. However, the thickness used for the fracture stress calculation was as follows:

(1) Cylindrical bending test - the minimum thickness in the test orientation.

(2) Biaxial flexure strength - the thickness at the center.

(3) Four-point twisting - the minimum thickness at the edge of the specimen.

For specimens undergoing cylindrical bending and biaxial strength tests, scotch tape was applied on the compressive surface of the test specimen to retain segments after fracture. Tape was not used on specimens subjected to 4-point twisting, since shear stress existed on both surfaces.

The deflection of each cell during testing was monitored by an extensometer* and recorded on an x-y plotter.** The load was applied by an Instron Testing Machine*** with loading rate 0.1 in./min and chart speed 2 in./min. Detailed results for each test are given in Appendix B in Tables B-1 to B-18.

To make meaningful correlation of these data, the measured strengths for each test sequence were presented in a Weibull plot describing probability of failure as a function of strength. The caracteristics of these plots are illustrated and discussed in the following section.

---

* Strain Gage Extensometer, G51-12A, range: 0-0.500 in., Instron Corporation, Canton, MA.

** X-Y Recorder, Model 135A, F. L. Moseley Co., Pasadena, CA.

***Instron Corporation, Model 1122, Canton, MA.

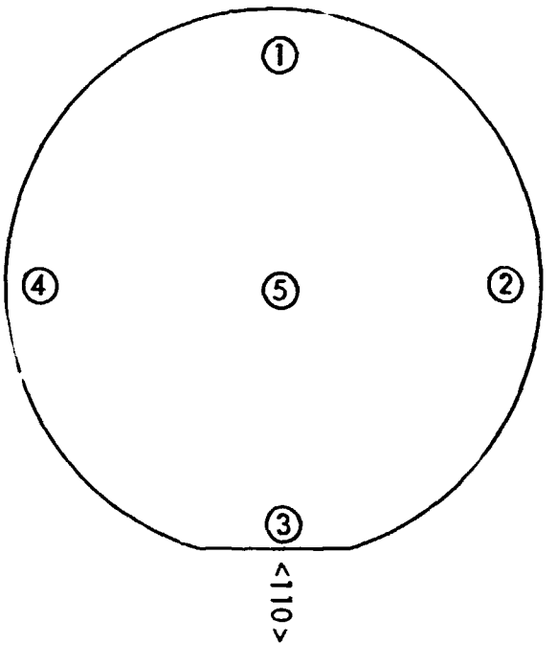


Figure 4-4. Locations of Specimen Cell Thickness Measurement

## SECTION V

## DISCUSSION OF TEST RESULTS

### A. EFFECT OF TEST METHODS ON STRENGTH DATA OF SILICON WAFERS

As-cut and chemically polished wafers under four-point twisting, uniaxial MOR and biaxial strength were used to evaluate the effect of test methods on the strength of wafers. Weibull plots of these strength data are shown in Figure 5-1. In this figure, the strengths of as-cut wafers at 50% failure probability under twist, MOR, and biaxial stresses are approximately 93, 117, and 194 $MNm^{-3}$ (14, 17, and 28) ksi), respectively. Similarly, the strengths of chemically polished wafers at 50% failure probability are 217, 278, and 496 $MNm^{-2}$ (31, 40, and 72 ksi) for twist, MOR, and biaxial stresses, respectively. As mentioned before, the larger the surface area of the sample under stress, the greater the probability that the largest flaw will be under stress. The four-point twisting test can stress almost the entire wafer area; cylindrical bending to determine the MOR strength can stress less than 30% of the wafer surface and edge, while the biaxial strength test stresses only 10% of the surface area at the center and none of the specimen's edge. Therefore, the measured strength under biaxial stress is much higher than that under cylindrical bending or twisting. The twist strength of as-cut wafers is the lowest among these three methods.

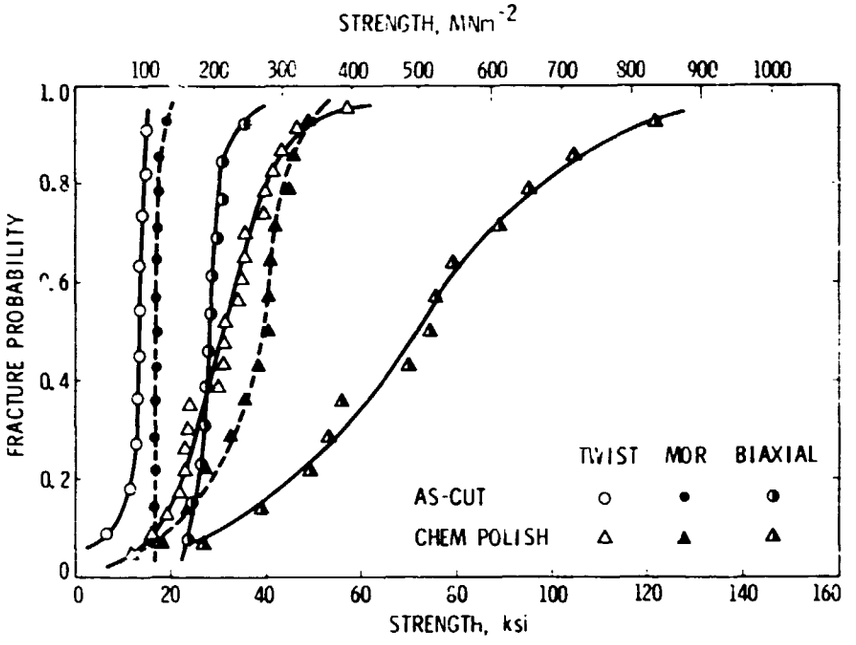


Figure 5-1. Effect of Test Methods on the Measured Strength of Silicon Wafers

## B. EFFECT OF CRYSTALLINE ORIENTATION ON THE MOR OF SILICON WAFERS

As-cut and chemically polished wafers under cylindrical bending are used to evaluate the effect of crystalline orientation on the strength of silicon wafers. Cylindrical bending was used here as it is highly directional in its stress application. Weibull plots for as-cut wafers tested in <100> and <110> orientations are shown in Figure 5-2. The plots for chemically polished wafers in <110> and 22.5° off <110> (half way between <100> and <110>), respectively, are also shown in Figure 5-2. It can be seen that the Weibull distributions of MOR for as-cut wafers in <100> and <110> orientations are very close A similar relationship exists between the Weibull distributions for chemically polished wafers in <110> and 22.5° off <110>. Therefore, the effect of crystalline orientation on the strength of silicon solar cell does not appear to be significant.

The typical fracture modes of silicon wafers subjected to cylindrical bending is shown in Figure 5-3. The fracture of wafers under <110> bending is found to be in {111} planes at <110> direction; under <100> bending cracking is found in {111} planes in <110> orientations and ziz-zags in the <100> loading direction. These fracture modes and lack of sensitivity to crystallographic orientation suggest that the strength of silicon wafers is controlled by crack initiation but not crack propagation. The fracture origin of tested cells was examined and found to be edge flaws. The quantitative measurement of the critical flaw size of each sample is beyond the scope of the present report.

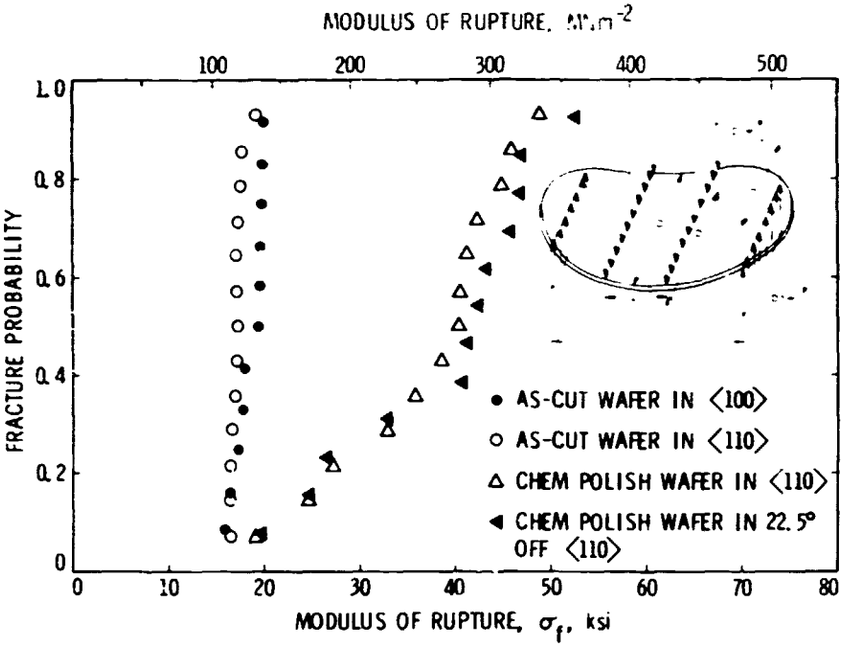


Figure 5-2. Effect of Crystailine Orientations on Modulus of Rupture Strength of As-cut and Chemically Polished Silicon Wafers

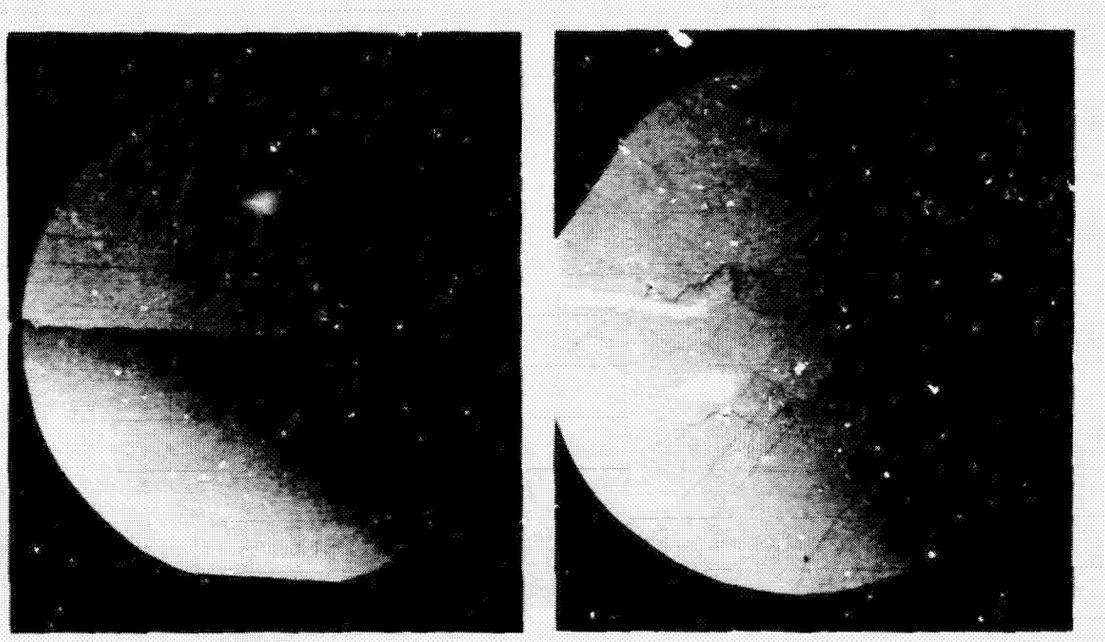


Figure 5-3. Fracture Modes of As-cut Wafers

The MOR value for chemically polished wafers at 50% fracture probability is approximately 278 $MNm^{-2}$ (40 ksi), which is more than twice the strength of as-cut wafers. Chemical polishing is shown to be effective in reducing surface flaws of wafers resulting from wafering. This subject will be discussed later.

## C. BIAXIAL STRENGTH OF SILICON WAFERS

The biaxial strength distributions of as-cut, chemically polished, and texture etched wafers are plotted in Figure 5-4. The biaxial strength at 50% fracture probability for as-cut wafers is 194 $MNm^{-2}$ (28 ksi) and that for chemically polished wafers is 49[illegible] $MNm^{-2}$ (72 ksi). A greater than twofold increase in strength results from chemical polishing, and a similar increase is seen for texture etching.

As can be seen in Figure 5-4, chemical polishing is more effective for reduction of the smaller surface flaws than of the larger flaws, such that a greater increase in strength is found at higher strengths than at the lower strength portion of the distribution curve. The thickness of chemically polished wafers was approximately 50 $\mu$m (~0.002 in.) smaller than that of as-cut wafers, suggesting that more extensive chemical polishing is necessary.

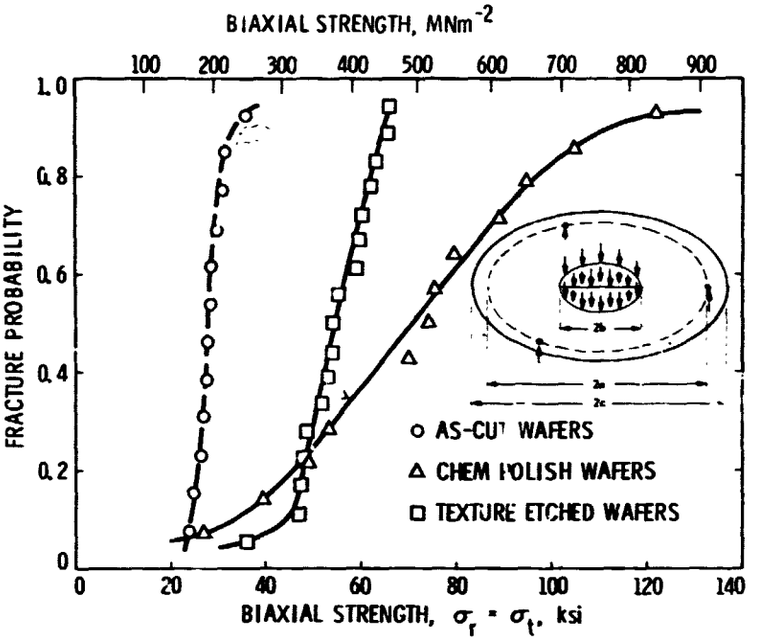


Figure 5-4. Biaxial Strength of Silicon Wafers

Texture etched wafers were produced by chemical etching from as-cut (with edge rounded) wafers. In this process, a dense population of tiny pyramids covering the entire surface of each cell was generated by chemical etching at the preferential crystalline direction. This pyramid-textured surface has been demonstrated to intercept the reflected sunlight and to increase cell performance.

The overall strength of texture etched wafers is greater than that of as-cut wafers (Figure 5-4) as a result of surface flaw reduction by etching. Although the mean strength of texture etched wafers is lower than that of chemically polished wafers, it should be pointed out that the strength of the wafers at low fracture probabilities is the region of interest. The texture teching has the effect of reducing large flaws and providing a more uniform distribution of small flaws associated with the roots of the pyramids. This leads to a more uniform breakage strength than does chemical polishing. Increased chemical polishing may, however, also improve this low-fracture probability region.

It should be noted that the strength of specimens under the biaxial stress test is controlled by the surface area confined within a small central region, whereas under cylindrical bending less than 30% of the total edge and surface area of the specimen is tested. Therefore, the surface condition of the specimen is important for biaxial strength measurement. Angle lapping was used to determine the surface damage from these types of wafers. Microphotos of the angle lapped areas of typicl as-cut, chemically polished, and texture etched wafers are shown in Figure 5-5. The average depth of surface damage is estimated to be 55, 35, and 40 $\mu$m for as-cut, chemically polished,

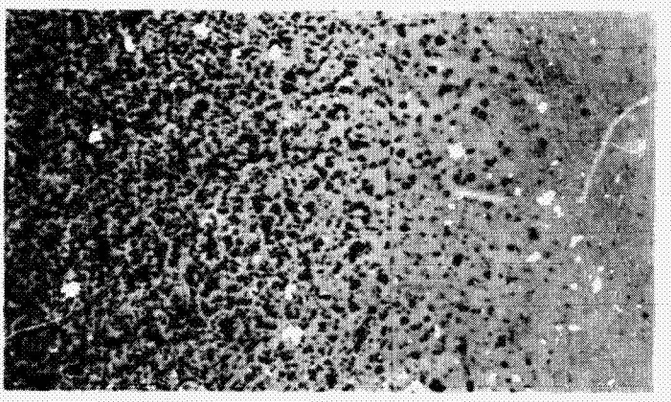

As-cut Wafer

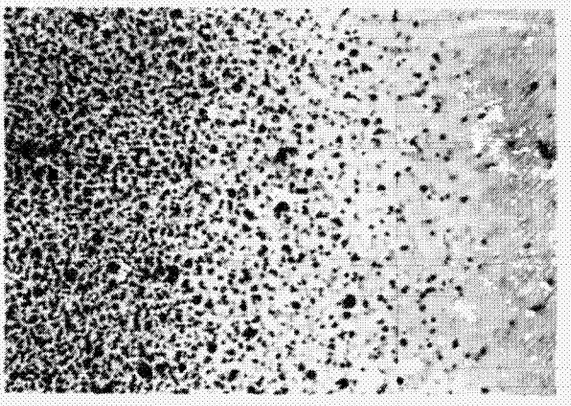

Chemically Polished Wafer

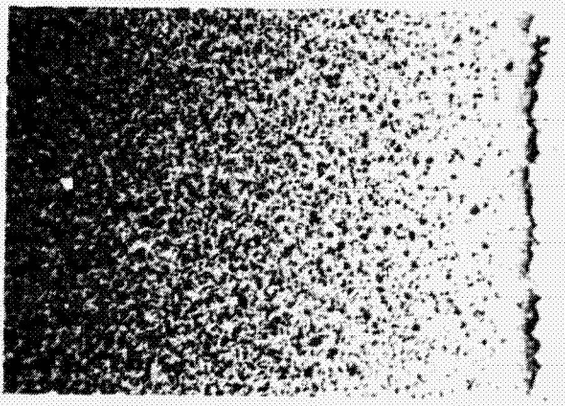

Texture Etched Wafer

Figure 5-5. Typical Angle Lapped Surface Areas for As-cut, Chemically Polished, and Texture Etched Wafers (Lapping angle is 2° 52')

and texture etched wafers, respectively. The average depth of surface damage correlates with the mean strength of these wafers.

The typical fracture modes of as-cut and chemically polished wafers subjected to the biaxial flexture test are shown in Figure 5-6. The fracture of silicon wafers was found to be initiated at the center of the specimen where the maximum biaxial stress occurred under this test configuration. Much finer segments resulted from the fracture of chemically polished samples than from as-cut samples. The measured strength of chemically polished wafers is greater than that of as-cut samples; thus more energy is available to initiate a larger number of cracks simultaneously.

## D. EFFECT OF CELL PROCESSES ON THE TWIST STRENGTH OF WAFERS

As discussed in Section III C, the four-point twisting test was recommended to be a standard method for testing the mechanical strength of silicon solar cells. The twist strengths of silicon wafers at several cell process steps are shown in Figure 5-7. Figure 5-8 compares the strength of the completed (metallized) cell with that of the end items of several preceding process steps. The following observations have emerged from twist strength data recorded at various process steps in the production of silicon cells:

1. The twist strengths of both as-cut and edge rounded wafers at 50% fracture probability are the same: 93 $MNm^{-2}$ (13.5 ksi). The Weibull distributions for these two types of wafers are also

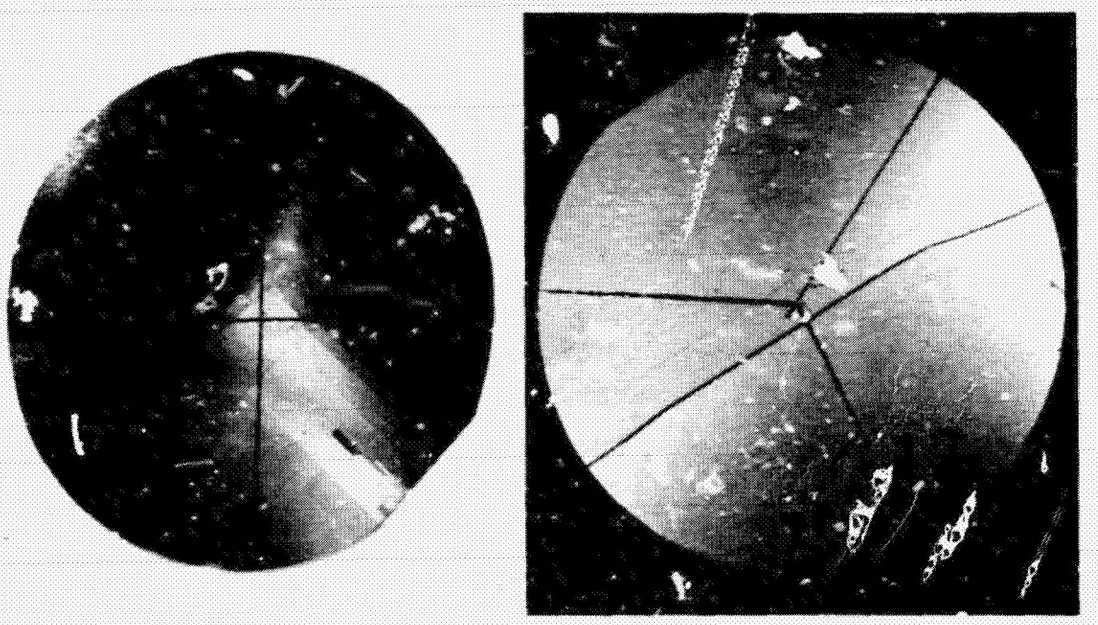

Chemically Polished As-cut

Figure 5-6. Typical Fracture Modes of As-cut and Chemically Polished Wafers Subjected to Biaxial Flexure Test

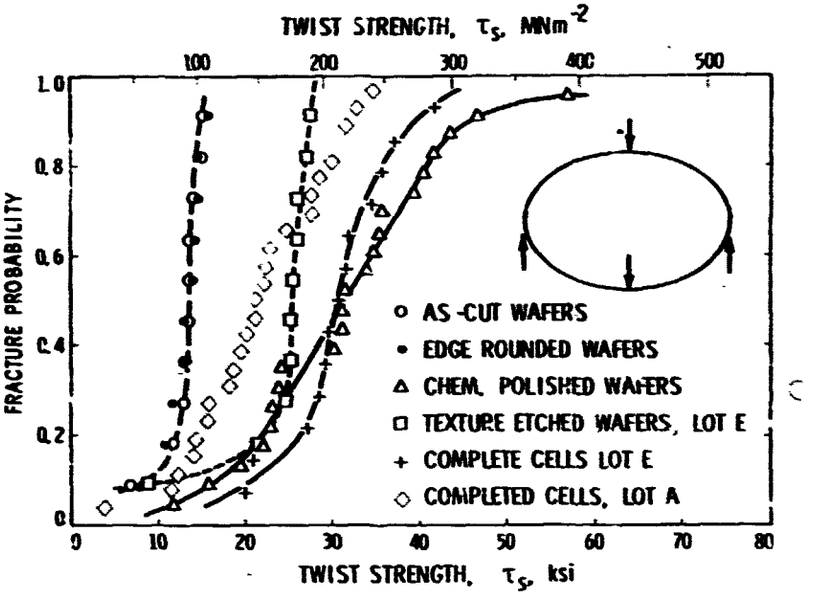


**Figure 5-7. Effect of Cell Processes on the Twist Strength of Silicon Wafers and Cells**

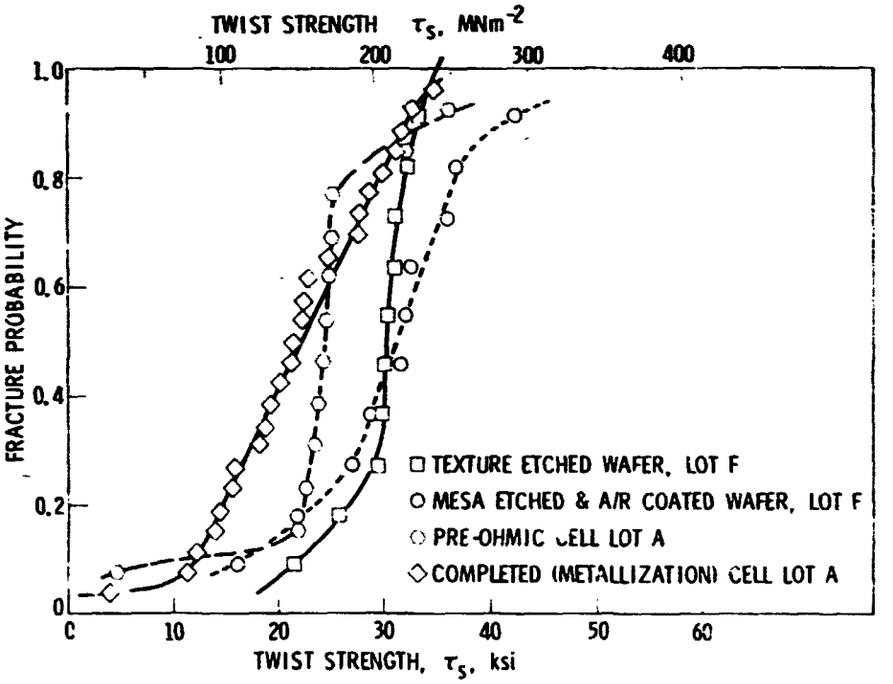


**Figure 5-8. Effect of Metallization and Other Cell Processes on the Strength of Solar Cells**

identical. The mechanical edge rounding method produces no increase in the strength of silicon wafers. The manufacturer has reported that edge rounding has been used to reduce cell cracking from edge corner damage occurring during cell processing and handling. An improved edge-rounding method that can remove edge corners and flaws and increase the strength of silicon wafers needs to be developed.

2. The twist strength of chemically polished wafers at 50% fracture probability is 217 $MNm^{-2}$ (31.5 ksi), which is more than twice the strength of as-cut wafers. Similar results were obtained from the cylindrical bending and biaxial strength tests (Figures 5-3 and 5-4, respectively). A reduction of flaw size must occur during the chemical etching process, since the strength of wafers is controlled by the critical flaw size. Chemical polishing appears to be more effective in reducing smaller flaws than larger flaws; the slope of the Weibull plot for the strength of chemically polished wafers is smaller than that for as-cut wafers. This implies that more etching on the wafer edge may be necessary to further eliminate the large flaws and improve the strength of silicon wafers.

3. The twist strength of texture etched wafers lot E at 50% fracture probability is 176 $MNm^{-2}$ (25.5 ksi), which is higher than that of as-cut wafers. This suggests that texture etching is effective in improving the strength of wafers. As discussed before, texture etching reduces the surface damage from ingot cutting. It is of importance to note that a tail below 20% fracture probability on the strength distribution curve is usually found in each strength measurement of wafers. As seen in Figure 5-7, an appreciable long tail in the minimum strength end of the curve is found for this lot of texture etched wafers. Texture etched wafers that fail below the 20% fracture probability curve are particularly vulnerable to fracture during subsequent cell processing and handling. Proof testing is useful for truncating the strength distribution of ceramics (Reference 12). A proof test at a proper stress level can be implemented after texture etching to reduce cell fracture during subsequent cell processes.

4. The twist strength of completed cells (lot E) at 50% fracture probability is 214 $MNm^{-2}$ (31 ksi). These cells were fabricated from the same lot as the texture etched wafers. As in Figure 5-7 the strength of completed cells appears to be increased by metallization.

5. A twist strength distribution of completed cells (lot A) is also plotted in Figure 5-7. The strength of these completed cells is lower than that of texture etched wafers. No detailed information on the cell process is available. Preliminary examination indicated that chips and flaws were present on the cells of lot A. Figure 5-9 shows an example of cell cracking originating from an edge chip. Quantitative measurements of edge chips and surface flaws and correlation with the strength of cells will be made later. It is likely that chips and flaws are generated from cell processing and handling. A rather small slope and a long tail are seen at the low stress points of the strength distribution curve of cell lot A. Cells

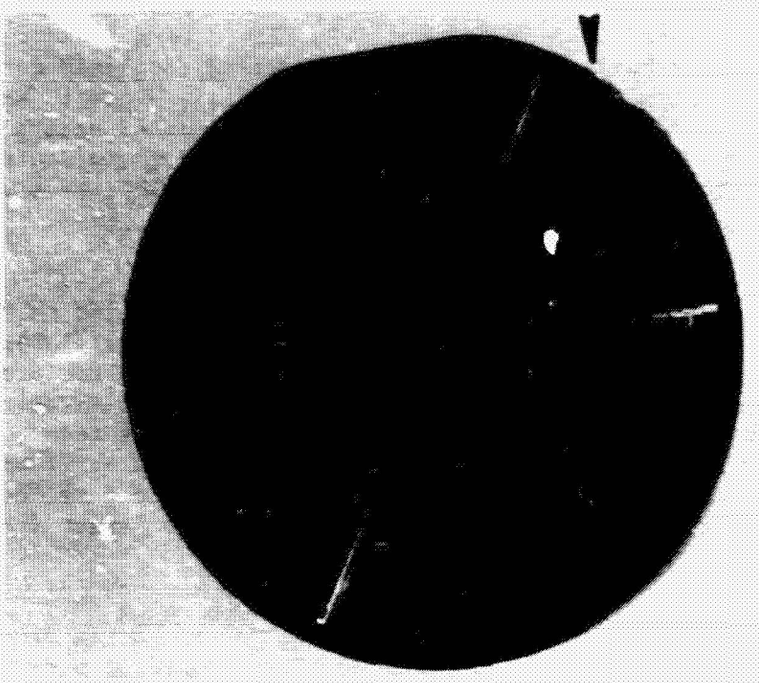

Figure 5-9. Typical Fractured Cell with Edge Chip

which fail at the low stresses of the distribution curve are more likely to crack during subsequent panel assembly, QA testing, and/or field service. Proof tests may be used to screen out weak cells prior to panel assembly.

6. The comparison of the strength of mesa etched and anti-reflection (A/R) coated wafers with that of texture etched wafers of the same lot (lot F) is shown in Figure 5-8. Mesa etching and A/R coating tends to increase strength slightly at the higher stress levels, suggesting that mesa etching and A/R coating processes are not effective in reducing large surface flaws.

7. The comparison of the strength of pre-ohmic cells and that of completed cells of the same lot (lot A) is shown in Figure 5-8. The twist strengths at 50% fracture probability for pre-ohmic cells and completed cells are approximately 172 $MNm^{-2}$ (25 ksi) and 152 $MNm^{-2}$ (22 ksi), respectively. Completed cells were processed from pre-ohmic patterned cells by putting on metallization. The major metallization processes of this manufacturer include palladium silicide, electroless nickel plating, and Sn-Pb soldering. The total thickness of this metallization is approximately 0.1 mm. The strength of completed metallized cells should be greater than that of pre-ohmic cells. As seen in Figure 5-8, however, the strength of completed (metallized) cells was found to be lower than that of pre-ohmic cells at most stress levels of the strength distribution curves. This observation is the opposite of the expectation. As previously described, edge

chips and surface flaws are related to the weakening of the completed cell lot A. These chips and flaws were apparently extended and generated by the metallization process. It should be pointed out that both strength distribution curves of pre-ohmic and completed cells have long tails extending to the low stress levels. Since it appears that the large critical flaws obtained in a cell process step are carried on to the subsequent processes, extension of these flaws under stress is expected. Proof tests should be used to eliminate those wafers and cells of the lower strength at the early stages of processing.

8. As mentioned in Section IV C, scotch tape was applied on the compressive surface of test specimens undergoing cylindrical bending and biaxial strength tests to retain the segments after fracture. Tape was not used on specimens undergoing the four-point twisting test, since shear stress existed on both surfaces of the test specimen; therefore, those specimens shattered as shown in Figure 5-10. Specimens which fractured into smaller fragments were found to have greater strength than those which fractured into larger fragments.

## E. EFFECT OF LOTS ON THE STRENGTH OF WAFERS AND CELLS

Several lots of texture etched wafers and completed cells were tested to determine the effect of lot numbers on the strength of wafers and cells. The twist strengths of texture etched wafers of several lots are plotted in Figure 5-11. The twist strengths of completed cells of several lots are shown in Figure 5-12. Appreciable strength variations were observed among lots for both texture etched wafers and completed cells. It should be pointed out that Lot E of the texture etched wafers has a long tail in the low strength end of the distribution curve while Lots B and F show very small scatter in strength data, as shown in Figure 5-11. This implies that proper texture etching may be able to increase the strength of silicon wafers. More studies need to be done to elucidate the effect of texture etching on the strength of silicon wafers. However, improved control of process procedures and better handling during processing should reduce the variations in mechanical strength of solar cells among lots.

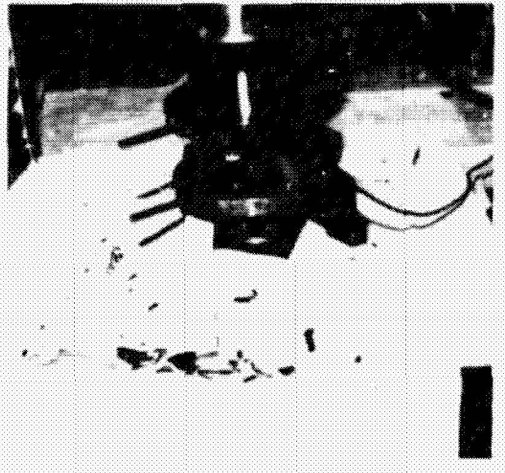

Shatter

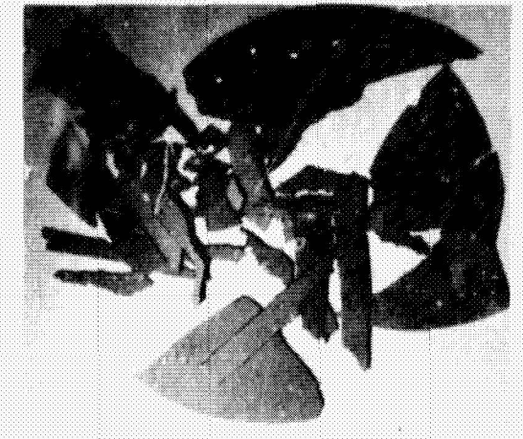

Small Fragments

Large Fragments

Figure 5-10. Typical Fractures of Silicon Wafers Subjected to Four-point Twisting

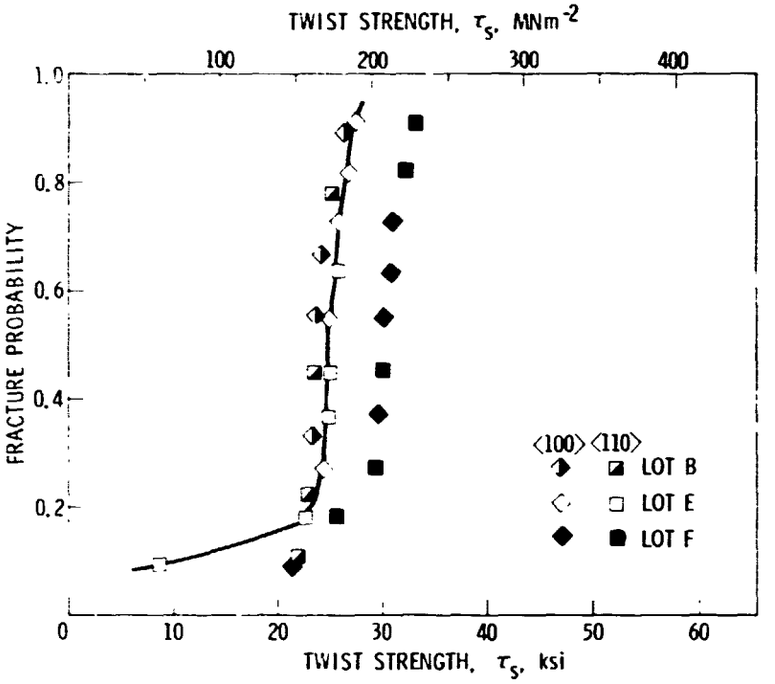


**Figure 5-11. Effect of Lots on Twist Strength of Texture Etched Wafers**

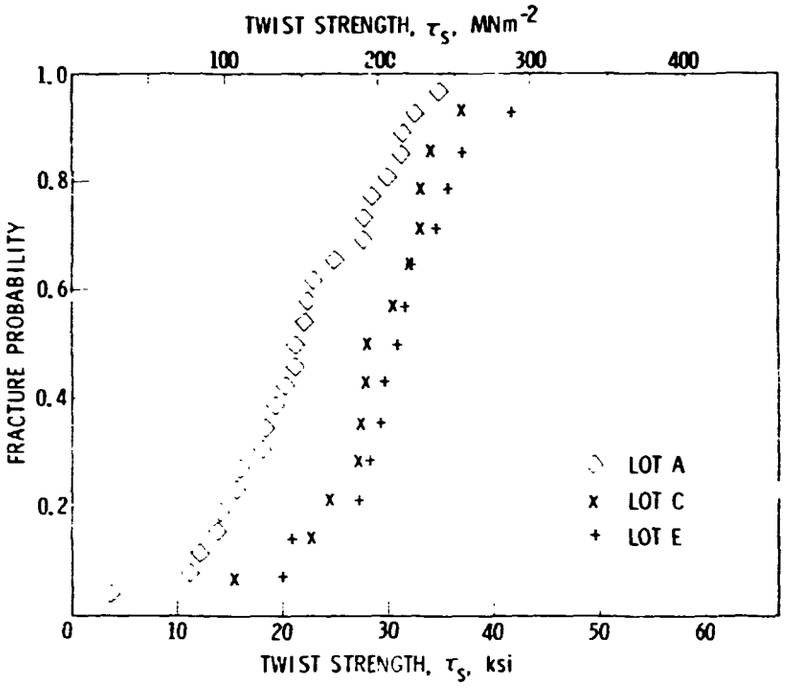


Figure 5-12. Effect of Lots on Twist Strength of Completed Cells

## SECTION VI

## CONCLUSIONS

The following conclusions have been drawn from the results of this test program:

1. The four-point twisting test is recommended as a standard test method for measurement of the mechanical strength of silicon solar cells because it has the following advantageous characteristics:

   (a) Simple loading configuration

   (b) Self-alignment

   (c) Symmetrical

   (d) Easy to perform

   (e) Stresses almost the entire cell specimen, including the edge

2. The Weibull distribution plot of strength data is useful to describe the strength characteristics of each type of wafer or cell at various cell process steps and to describe the flaw distribution of each sample type.

3. The effect of crystalline orientation on the strength of silicon solar cells is small, since the strength of a silicon wafer is controlled by crack initiation but not crack propagation.

4. Chemical polishing is useful for reducing the surface flaws of silicon wafers. A greater than twofold increase in mean strength of wafers results from chemical polishing. However, it is more effective in the reduction of the smaller flaws than of larger flaws. A greater increase in strength is found at higher strengths than at the lower strength portion of the distribution curve.

5. Texture etching reduces somewhat the surface damage resulting from ingot cutting, so that the overall strength of a textured wafer is higher than that of an as-cut wafer, although the mean strength of texture etched wafers is lower than that of chemically polished wafers.

6. Mechanical edge rounding does not produce significant change in the strength of the silicon wafer.

7. Mesa etching and anti-reflection coating of wafers and pre-ohmic (patterned) cells result in little change in strength from the prior process.

8. The strength of wafers and cells varied from lot to lot. Edge flaws in samples which were generated during processing and handling were found to be the controlling factor in the measured strength of samples in a lot.

9. A long tail at the low stress portion of the strength distribution curve was found for several types of samples. The wafers or cells in the low strength distribution are likely to be fractured during subsequent cell processing and handling or in the field service. A proof test would be useful to eliminate these samples before the subsequent cracking occurs.

## SECTION VII

## RECOMMENDATIONS

The information presented in this report is the result of work carried out during the first phase of a continuing effort to evaluate the fracture strength of silicon solar cells. The recommendations that follow are of further work to be carried out during the second phase of his test program to generate additional information important for engineering design use. The recommendations are:

(1) Continue and complete the Weibull statistical analysis of the present strength data on silicon solar cells.

(2) Design and fabricate a four-point twisting test jig adjustable for various sizes (e.g., up to 6-inches in diameter) and shapes (e.g., square, rectangular) of solar cells.

(3) Investigate the four-point twisting method in more detail analytically and experimentally.

(4) Perform further tests of cell physical characteristics on cells from various manufacturers to determine important fracture-controlling factors such as edge and surface conditions resulting from various wafering and processing, as well as the nature of sheet, shape, size, etc.

(5) Conduct failure analysis to determine the nature and source of the flaw controlling the fractur of solar cells.

(6) Establish proof test levels for critical cell processes.

(7) Determine QA procedures and mechanical strength criteria for silicon solar cells.

(8) Evaluate the effect of chemical polishing and texture etching on the strength of silicon wafers.

(9) Evaluate tearing fracture properties of silicon by measuring the critical stress-intensity factor for Mode III crack extension or $K_{III\ C}$.

## REFERENCES


1. Anhalt, K. J., "Quality Assurance, Block III: Experience to March 1, 1979," presented at Low-Cost Solar Array Project 12th Project Integration Meeting, California Institute of Technology, Pasadena, CA, April 4-5, 1979.

2. Shumka, A. and K. H. Stern, "Some Failure Modes and Analysis Techniques for Terrestrial Solar Cell Modules," Proceedings of 13th IEEE Photovoltaic Specialists Conference, pp. 824-34, Washington, D.C., June 5-8, 1978.

3. Weibull W., "The Phenomenon of Rupture in Solids," Ingeniors Vetenskaps Akademiens, Handlingar, Vol. 153, pp. 1-55, (1939).

4. Weibull, W., "A Statistical Distribution Function of Wide Applicability," J. Appl. Mech., Vol. 18, pp. 293-297, (1951).

5. ASTM C 158-72, "Standard Methods of Flexure Testing of Glass (Determination of Modulus of Rupture)."

6. Giovan, M. N., "An Experimental and Statistical Study of the Uniaxial and Equibiaxial Strength of a Brittle Material," M. S. Thesis in Engineering, UCLA, 1978.

7. ASTM F394-74T, "Tentative Test Method for Biaxial Flexure Strength (Modulus of Rupture) of Ceramic Substrates."

8. Vitman, F. F., Bartenev, G. M., Pukh, V. P., and L. P. Tsepkov, "A Method for Measuring the Strength of Sheet Glass," Steklo i Keramika, Vol. 19, No. 8, pp. 9-11, August 1962.

9. Wachtman, J. B., Jr., Capps, W. and J. Mandel, "Biaxial Flexure Tests of Ceramic Substrates," J. of Materials, Vol. 7, No. 2, pp. 188-94, (1972).

10. Kirstein, A. F. and R. M. Wooley, "Symmetrical Bending of Thin Circular Elastic Plates on Equally Spaced Point Supports," J. of Research, (National Bureau of Standards), Vol. 71C, No. 1, pp. 1-10, (1967).

11. Peery, D. J., Aircraft Structures, Chapter 13, McGraw-Hill, 1960.

12. Wiederhorn, S. M. and N. J. Tighe, "Proof-testing of Hot-Pressed Silicon Nitride," J. Matl. Science, Vol. 13, pp. 1781-93, (1978).

## APPENDIX A

## STRESS CALCULATION OF TEST CONFIGURATIONS

### 1. Cylindrical Bending

The loading condition of a cell under cylindrical bending is shown in Figure 3-1. The fiber stress or modulus of rupture (MOR) can be calculated by

$$\sigma = \frac{3P(L-\ell)}{2\,d\,t^2} \qquad \text{(A-1)}$$

where

P = total applied force

L = outer span

$\ell$ = center span

t = thickness of the cell specimen

d = width of the beam under stress. In this case, d is the chord length of the cell specimen parallel to the loading line, varying from inner loading line length D' to diameter D, depending upon the location of the fracture originating flaw (as shown in Figure 3-1).

For a 76 mm (3 in.) diameter cell in which $\ell$ is 25.4 mm (1 in.), D' is calculated to be 71 mm (2.8 in.). The difference between D and D' is small. Therefore, the MOR value of a cell under cylindrical bending can be calculated approximately by

$$\sigma = \frac{3P(L-\ell)}{2\,D\,t^2} \qquad \text{(A-2)}$$

### 2. Biaxial Flexure Strength

This loading condition is shown in Figure 3-2. The maximum radial and tangential stresses ($\sigma_{r_{max}}$ and $\sigma_{t_{max}}$, respectively) can be calculated (Reference 9) by

$$\sigma_{r_{max}} = \sigma_{t_{max}} = -\frac{3}{4\pi}\,\frac{P}{t^2}\,(X - Y) \qquad \text{(A-3)}$$

where

$$X = (1 + \nu) \ln\left(\frac{b}{c}\right)^2 + \frac{1 - \nu}{2}\left(\frac{b}{c}\right)^2$$

$$Y = (1 + \nu)\left[1 + \ln\left(\frac{a}{c}\right)^2\right] + (1 - \nu)\left(\frac{a}{c}\right)^2$$

In these equations,

c = radius of the specimen

a = radius of the concentric circle of supporting points

b = radius of the loaded area of the specimen

$\nu$ = Poisson's Ratio

3. Four-Point Twisting

A stress analysis of a rectangular cross-sectional member subjected to a torsion, T, the maximum shear stress, $\tau_s$, can be calculated by an equation (Reference 11) as

$$\tau_s = \frac{T}{\alpha d\, t^2} \qquad \text{(A-4)}$$

where

$\alpha$ = a constant which is a function of b/t,

d = width of the specimen

A cell specimen subjected to four-point twisting is shown schematically in Figure 3-3. In this case, the applied torsional moment, T, is given by the expression

$$T = \frac{P}{2} s \qquad \text{(A-5)}$$

where

P is the total fracture force

s is the distance between the torsional forces.

Since a solar cell is a very thin disc, the ratio $b/t \to \infty$. Therefore (Reference 11) $\alpha = 1/3$, and it can be approximated that

$$d \approx s$$

Substituting these values and Equation A-5 into Equation A-4, the twist (shear) stress can be estimated by

$$\tau_s = \frac{3P}{2t^2} \qquad \text{(A-6)}$$

## APPENDIX B

## MEASURED CELL STRENGTH DATA

As-cut and chemically polished silicon wafers were used to evaluate the modulus of rupture (MOR) strength of silicon in several crystalline orientations using the cylindrical bending test. The results for as-cut wafers undergoing the cylindrical bending test in <100> and <110> orientations are given in Tables B-1 and B-2, respectively. The results for chemically polished wafers undergoing cylindrical bending in <110> and 22.5° off <110> (direction halfway between <100> and <110> orientations) are given in Tables B-3 and B-4, respectively. The test results for as-cut, chemically polished, and edge rounded wafers are given in Tables B-8, B-9, and B-10, respectively.

As-cut, chemically polished, and texture etched silicon wafers were evaluated by their performance in the biaxial flexure strength test. The results are given in Tables B-5, B-6, and B-7, respectively.

The four-point twisting test was used to evaluate the twist strength of wafers and cells as a function of cell process steps. The test results for as-cut, chemically polished, and edge rounded wafers are given in Tables B-8, B-9, and B-10, respectively. The effect of lots on the twist strength test results for texture etched wafers is given in Tables B-11 to B-13. The results for mesa etched and A/R coated wafers and pre-ohmic cells under four-point twisting are given in Tables B-14 and B-15, respectively. The twist strength test results for completed cells of several lot numbers are given in Tables B-16 to B-18.

**Table B-1. Results of As-Cut Wafers Under Cylindrical Bending Tests in <100>**

| Specimen No. | Fracture Force (lb) | Minimum Thickness (in.) | Center Deflection at Failure (in.) | Fracture Stress (psi) |
|---|---|---|---|---|
| 1-57 | 8.9 | 0.0171 | 0.055 | 17,745 |
| 1-58 | 8.9 | 0.0173 | 0.055 | 17,337 |
| 1-59 | 8.1 | 0.0172 | 0.047 | 15,962 |
| 1-60 | 9.9 | 0.0172 | 0.058 | 19,510 |
| 1-61 | 10.0 | 0.0172 | 0.057 | 19,707 |
| 1-62 | 10.0 | 0.0171 | 0.058 | 19,938 |
| 1-63 | 9.1 | 0.0171 | 0.055 | 18,143 |
| 1-64 | 8.3 | 0.0171 | 0.048 | 16,548 |
| 1-65 | 10.0 | 0.0171 | 0.058 | 19,938 |
| 1-66 | --* | 0.0172 | -- | -- |
| 1-67 | 10.3 | 0.0172 | 0.059 | 20,298 |
| 1-68 | 9.9 | 0.0172 | 0.059 | 19,510 |

*Failed before test.

**Table B-2. Results of As-Cut Wafers Under Cylindrical Bending Tests in <110>**

| Specimen No. | Fracture Force (lb) | Minimum Thickness (in.) | Center Deflection at Failure (in.) | Fracture Stress (psi) |
|---|---|---|---|---|
| 1-44 | 8.7 | 0.0173 | 0.057 | 16,947 |
| 1-45 | 9.0 | 0.0175 | 0.054 | 17,133 |
| 1-46 | 8.6 | 0.0174 | 0.046 | 16,560 |
| 1-47 | 9.1 | 0.0173 | 0.050 | 17,726 |
| 1-48 | 10.0 | 0.0174 | 0.047 | 19,256 |
| 1-49 | 9.0 | 0.0174 | 0.046 | 17,330 |
| 1-50 | 8.8 | 0.0173 | 0.051 | 17,142 |
| 1-51 | 8.4 | 0.0173 | 0.040 | 16,363 |
| 1-52 | 8.2 | 0.0171 | 0.040 | 16,349 |
| 1-53 | 8.3 | 0.0172 | 0.043 | 16,356 |
| 1-54 | 8.9 | 0.0172 | 0.044 | 17,539 |
| 1-55 | 8.7 | 0.0172 | 0.042 | 17,145 |
| 1-56 | 8.7 | 0.0172 | 0.045 | 17,145 |

**Table B-3. Results of Chemically Polished Wafers Under Cylindrical Bending in <110>**

| Specimen No. | Fracture Force (lb) | Minimum Thickness (in.) | Center Deflection at Failure (in.) | Fracture Stress (psi) |
|---|---|---|---|---|
| 3-57 | 10.6 | 0.0151 | 0.077 | 27,103 |
| 3-58 | 18.8 | 0.0150 | 0.136 | 48,713 |
| 3-59 | 15.8 | 0.0151 | 0.108 | 40,399 |
| 3-60 | 17.7 | 0.0150 | 0.123 | 45,863 |
| 3-61 | 13.8 | 0.0150 | 0.088 | 35,757 |
| 3-62 | 15.9 | 0.0150 | 0.118 | 41,199 |
| 3-63 | 12.3 | 0.0148 | 0.102 | 32,738 |
| 3-64 | 16.3 | 0.0150 | 0.113 | 42,235 |
| 3-65 | 17.3 | 0.0150 | 0.119 | 44,826 |
| 3-66 | 15.6 | 0.0150 | 0.117 | 40,421 |
| 3-67 | 15.1 | 0.0151 | 0.107 | 38,609 |
| 3-68 | 9.3 | 0.0148 | 0.066 | 24,753 |
| 3-69 | 7.3 | 0.0149 | 0.054 | 19,170 |

**Table B-4. Results of Chemically Polished Wafers Under Cylindrical Bending in 22.5° <110>**

| Specimen No. | Fracture Force (lb) | Minimum Thickness (in.) | Center Deflection at Failure (in.) | Fracture Stress (psi) |
|---|---|---|---|---|
| 3-70 | 9.0 | 0.0146 | 0.076 | 24,615 |
| 3-71 | 15.3 | 0.0148 | 0.117 | 40,723 |
| 3-72 | 20.3 | 0.0150 | >0.137 | 52,600 |
| 3-73 | 7.6 | 0.0150 | 0.062 | 19,692 |
| 3-74 | 12.7 | 0.0150 | 0.108 | 32,907 |
| 3-75 | 15.7 | 0.0147 | 0.128 | 42,35· |
| 3-76 | 16.2 | 0.0148 | 0.129 | 43,118 |
| 3-77 | 15.5 | 0.0148 | 0.125 | 41,255 |
| 3-78 | 18.1 | 0.0150 | >0.137 | 46,899 |
| 3-79 | 17.7 | 0.0150 | 0.129 | 45,863 |
| 3-80 | 17.9 | 0.0149 | 0.132 | 47,006 |
| 3-81 | 10.1 | 0.0149 | --* | 26,523 |

*Extensometer malfunction.

**Table B-5. Results As-Cut Wafers Under Biaxial Strength Test**

| Specimen No. | Fracture Force (lb) | Center Thickness (in.) | Center Deflection at Failure (in.) | Fracture Stress (psi) |
|---|---|---|---|---|
| 1-32 | 7.6 | 0.0178 | -- | 35,740 |
| 1-33 | 5.2 | 0.0179 | -- | 24,181 |
| 1-34 | 6.1 | 0.0178 | 0.062 | 28,686 |
| 1-35 | 5.9 | 0.0179 | 0.053 | 27,437 |
| 1-36 | 5.2 | 0.0178 | 0.050 | 24,454 |
| 1-37 | 5.9 | 0.0178 | 0.055 | 27,746 |
| 1-38 | 6.0 | 0.0177 | 0.052 | 28,536 |
| 1-39 | 6.6 | 0.0178 | 0.055 | 31,038 |
| 1-40 | 5.6 | 0.0178 | 0.050 | 26,335 |
| 1-41 | 5.6 | 0.0175 | 0.047 | 27,246 |
| 1-42 | 6.3 | 0.0177 | 0.052 | 29,963 |
| 1-43 | 6.5 | 0.0176 | 0.052 | 31,266 |

**Table B-6. Results of Chemically Polished Wafers Under Biaxial Strength Test**

| Specimen No. | Fracture Force (lb) | Center Thickness (in.) | Center Deflection at Failure (in.) | Fracture Stress (psi) |
|---|---|---|---|---|
| 3-44 | 4.6 | 0.0159 | 0.053 | 27,111 |
| 3-45 | 8.6 | 0.0155 | 0.080 | 53,336 |
| 3-46 | 19.4 | 0.0154 | 0.167 | 121,884 |
| 3-47 | 11.8 | 0.0154 | 0.115 | 74,136 |
| 3-48 | 9.0 | 0.0155 | 0.100 | 55,817 |
| 3-49 | 6.6 | 0.0158 | 0.080 | 39,393 |
| 3-50 | 8.2 | 0.0157 | 0.085 | 49,568 |
| 3-51 | 11.3 | 0.0155 | 0.110 | 70,081 |
| 3-52 | 16.9 | 0.0155 | 0.140 | 104,812 |
| 3-53 | 12.5 | 0.0153 | 0.120 | 79,563 |
| 3-54 | 11.9 | 0.0153 | 0.115 | 75,744 |
| 3-55 | 14.9 | 0.0153 | 0.140 | 94,840 |
| 3-56 | 13.8 | 0.0152 | 0.132 | 88,998 |

**Table B-7. Results of Texture Etched Wafers (Edge Rounded) Under Biaxial Strength Test**

| Specimen No. | Fracture Force (lb) | Center Thickness (in.) | Center Deflection at Failure (in.) | Fracture Stress (psi) |
|---|---|---|---|---|
| 5-1 | 9.8 | 0.0175 | 0.080 | 47,680 |
| 5-2 | 13.2 | 0.0173 | 0.098 | 65,716 |
| 5-3 | 10.4 | 0.0173 | 0.080 | 51,776 |
| 5-4 | 11.0 | 0.0174 | 0.085 | 54,135 |
| 5-5 | 13.4 | 0.0174 | 0.100 | 65,947 |
| 5-6 | 12.9 | 0.0176 | 0.098 | 62,051 |
| 5-7 | 10.0 | 0.0175 | 0.080 | 48,653 |
| 5-8 | 7.4 | 0.0175 | 0.068 | 36,003 |
| 5-9 | 10.1 | 0.0176 | 0.078 | 48,583 |
| 5-10 | 12.1 | 0.0173 | 0.090 | 60,239 |
| 5-11 | 9.5 | 0.0173 | 0.075 | 47,295 |
| 5-12 | 12.4 | 0.0171 | 0.095 | 63,185 |
| 5-13 | 11.1 | 0.0175 | 0.088 | 54,005 |
| 5-14 | 10.8 | 0.0174 | 0.085 | 53,151 |
| 5-15 | 12.3 | 0.0176 | 0.090 | 59,165 |
| 5-16 | 12.4 | 0.0176 | 0.093 | 59,646 |
| 4-17 | 11.6 | 0.0176 | 0.088 | 55,798 |

**Table B-8. Results of As-Cut Wafers Under Four-point Twisting**

| Specimen No. | Fracture Force (lb) | Minimum Thickness (in.) | Relative* Deflection at Failure (in.) | Fracture Stress $\tau_s$ (psi) |
|---|---|---|---|---|
| 1-11 | 4.5 | 0.0172 | 0.095 | 13,462 |
| 1-12 | --** | 0.0174 | -- | -- |
| 1-13 | 4.7 | 0.0172 | 0.083 | 14,060 |
| 1-14 | 4.3 | 0.0171 | 0.077 | 13,014 |
| 1-15 | 4.4 | 0.0169 | 0.083 | 13,634 |
| 1-16 | 4.5 | 0.0172 | 0.090 | 13,462 |
| 1-17 | 4.1 | 0.0176 | 0.078 | 11,714 |
| 1-18 | 4.9 | 0.0170 | 0.091 | 15,005 |
| 1-19 | 2.2 | 0.0170 | 0.052 | 6,737 |
| 1-20 | 5.0 | 0.0171 | 0.088 | 15,133 |
| 1-21 | 4.2 | 0.0171 | 0.077 | 12,712 |

*Relative deflection between two pairs of twisting forces.
**Specimen failed before test.

**Table B-9. Results of Chemically Polished Wafers Under Four-point Twisting**

| Specimen No. | Fracture Force (lb) | Minimum Thickness (in.) | Relative Deflection at Failure (in.) | Fracture Stress $\tau_s$ (psi) |
|---|---|---|---|---|
| 3-10 | 5.2 | 0.0142 | 0.137 | 22,823 |
| 3-11 | 9.9 | 0.0142 | 0.210 | 43,451 |
| 3-12 | 9.9 | 0.0145 | 0.210 | 41,678 |
| 3-13 | 8.3 | 0.0144 | 0.186 | 35,424 |
| 3-14 | 7.6 | 0.0147 | 0.146 | 31,126 |
| 3-15 | 2.8 | 0.0145 | 0.080 | 11,786 |
| 3-16 | 11.4 | 0.0147 | 0.215 | 46,689 |
| 3-17 | 9.4 | 0.0145 | 0.180 | 39,567 |
| 3-18 | 7.4 | 0.0145 | 0.160 | 31,149 |
| 3-19 | 4.7 | 0.0146 | 0.107 | 19,514 |
| 3-20 | 8.1 | 0.0145 | 0.170 | 34,095 |
| 3-21 | 3.9 | 0.0147 | 0.093 | 15,973 |
| 3-22 | 7.5 | 0.0145 | 0.145 | 31,570 |
| 3-23 | 5.9 | 0.0147 | 0.135 | 24,164 |
| 3-24 | 5.5 | 0.0145 | 0.177 | 23,151 |
| 3-25 | 7 | 0.0 47 | 0.176 | 35,631 |
| 3-26 | | 0.0143 | 0.125 | 22,072 |
| 3-27 | 0 | 0.0148 | 0.193 | 40,404 |
| 3-28 | .9 | 0.0147 | 0.256 | 56,928 |
| 3-29 | 5.4 | 0.0142 | 0.117 | 23,701 |
| 3-30 | 8.5 | 0.0147 | 0.180 | 34,812 |
| 3-31 | 7.2 | 0.0145 | 0.154 | 30,307 |

**Table B-10. Results of Edge Rounded Wafers Under Four-point Twisting**

| Specimen No. | Fracture Force (lb) | Minimum Thickness (in.) | Relative Deflection at Failure (in.) | Fracture Stress $\tau_s$ (psi) |
|---|---|---|---|---|
| 2-1 | 4.7 | 0.0171 | 0.125 | 14,225 |
| 2-2 | 4.9 | 0.0165 | 0.113 | 15,928 |
| 2-3 | 5.0 | 0.0175 | 0.100 | 14,449 |
| 2-4 | 2.8 | 0.0170 | 0.065 | 8,574 |
| 2-5 | 4.9 | 0.0172 | 0.105 | 14,658 |
| 2-6 | 3.8 | 0.0172 | 0.092 | 11,368 |
| 2-7 | 4.5 | 0170 | 0.100 | 13,780 |
| 2-8 | 4.1 | 0.0167 | 0.095 | 13,011 |
| 2-9 | 4.1 | 0.0167 | 0.093 | 13,011 |
| 2-10 | 3.5 | 0.0169 | 0.075 | 10,845 |

Table B-11. Results of Texture-Etched Wafers Lot B Under Four-point Twisting

| Specimen No. | Fracture Force (lb) | Minimum Thickness (in.) | Relative Deflection at Failure (in.) | Fracture Stress $\tau_s$ (psi) |
|---|---|---|---|---|
| 5-[illegible] | 7.5 | 0.0165 | 0.100 | 24,380 |
| 5-29 | 7.4 | 0.0166 | 0.103 | 23,766 |
| 5-30 | 7.7 | 0.0161 | 0.110 | 26,289 |
| 5-[illegible] | 7.2 | 0.0165 | 0.100 | 23,405 |
| 5-32 | 7.1 | 0.0165 | 0.115 | 23,080 |
| 5-33 | 6.8 | 0.0160 | 0.110 | 23,508 |
| 5-34 | 6.8 | 0.0165 | 0.110 | 22,105 |
| 5-35 | 7.5 | 0.0162 | 0.120 | 25,292 |

Table B-12. Results of Texture-Etched Wafers Lot E Under Four-point Twisting

| Specimen No. | Fracture Force (lb) | Minimum Thickness (in.) | Relative Deflection at Failure (in.) | Fracture Stress $\sigma_s$ (psi) |
|---|---|---|---|---|
| 5-38 | 7.8 | 0.0174 | 0.130 | 22,809 |
| 5-39 | 2.8 | 0.0168 | 0.063 | 8,780 |
| 5-40 | 8.9 | 0.0174 | 0.125 | 26,016 |
| 5-41 | 8.1 | 0.0169 | 0.127 | 25,099 |
| 5-42 | 8.0 | 0.0168 | 0.125 | 25,085 |
| 5-43 | 8.7 | 0.0169 | 0.150 | 26,958 |
| 5-44 | 8.5 | 0.0170 | 0.140 | 26,029 |
| 5-45 | 7.5 | 0.0164 | 0.145 | 24,678 |
| 5-46 | 8.3 | 0.0170 | 0.145 | 25,417 |
| 5-47 | 9.0 | 0.0170 | 0.143 | 27,561 |

**Table B-13. Results of Texture-Etched Wafers Lot F Under Four-point Twisting**

| Specimen No. | Fraction Force (lb) | Minimum Thickness (in.) | Relative Deflection at Failure (in.) | Fracture Stress $\sigma_s$ (psi) |
|---|---|---|---|---|
| 5-18 | 9.8 | 0.0167 | 0.135 | 31,098 |
| 5-19 | 9.5 | 0.0169 | 0.141 | 29,437 |
| 5-20 | 9.9 | 0.0170 | 0.135 | 30,317 |
| 5-21 | 6.6 | 0.0165 | 0.110 | 21,455 |
| 5-22 | 9.7 | 0.0166 | 0.135 | 31,153 |
| 5-23 | 10.6 | 0.0168 | 0.140 | 33,238 |
| 5-24 | 10.3 | 0.0168 | 0.155 | 32,297 |
| 5-25 | 8.6 | 0.0172 | 0.115 | 25,727 |
| 5-26 | 9.7 | 0.0170 | 0.140 | 29,704 |
| 5-27 | 9.4 | 0.0166 | 0.160 | 30,189 |

**Table B-14. Results of Mesa Etch and A/R Coated Wafers Lot F Under Four-point Twisting**

| Specimen No. | Fraction Force (lb) | Minimum Thickness (in.) | Relative Deflection at Failure (in.) | Fracture Stress $\tau_s$ (psi) |
|---|---|---|---|---|
| 6-1 | 13.2 | 0.0166 | 0.225 | 42,394 |
| 6-2 | 7.0 | 0.0169 | 0.135 | 21,690 |
| 6-3 | 11.5 | 0.0168 | 0.175 | 36,006 |
| 6-4 | 10.4 | 0.0170 | 0.155 | 31,848 |
| 6-5 | 8.95 | 0.0166 | 0.135 | 28,744 |
| 6-6 | 8.6 | 0.0168 | 0.155 | 26,966 |
| 6-7 | 10.6 | 0.0170 | 0.170 | 32,460 |
| 6-8 | 10.0 | 0.0167 | 0.155 | 31,733 |
| 6-9 | 5.15 | 0.0168 | 0.090 | 16,149 |
| 6-10 | 11.7 | 0.0168 | 0.183 | 36,687 |

Table B-15. Results of Pre-Ohmic Cells Lot A Under Four-point Twisting

| Specimen No. | Fracture Force (lb) | Minimum Thickness (in.) | Relative Deflection at Failure (in.) | Fracture Stress $\tau_s$ (psi) |
|---|---|---|---|---|
| 7-1 | 7.9 | 0.0168 | 0.125 | 24,771 |
| 7-2 | 8.2 | 0.0175 | 0.115 | 23,696 |
| 7-3 | 7.5 | 0.0168 | 0.118 | 23,517 |
| 7-4 | 8.2 | 0.0170 | 0.120 | 25,111 |
| 7-5 | 7.5 | 0.0165 | 0.133 | 24,380 |
| 7-6 | 7.5 | 0.0172 | 0.125 | 22,436 |
| 7-7 | 8.1 | 0.0169 | 0.137 | 25,099 |
| 7-8 | 7.1 | 0.0170 | 0.115 | 21,742 |
| 7-9 | 7.9 | 0.0170 | 0.113 | 24,192 |
| 7-10 | 11.6 | 0.0169 | 0.150 | 35,944 |
| 7-11 | 1.5 | 0.0169 | 0.040 | 4,648 |
| 7-12 | 10.3 | 0.0169 | 0.150 | 31,916 |

**Table B-16. Results of Completed Cells Lot A Under Four-point Twisting**

| Specimen No. | Fracture Force (lb) | Minimum Thickness (in.) | Relative Deflection at Failure (in.) | Fracture Stress $\tau_s$ (psi) |
|---|---|---|---|---|
| C-1 | 5.1 | 0.0170 | 0.090 | 15,618 |
| C-2 | 1.2 | 0.0168 | 0.035 | 3,763 |
| C-3 | 7.5 | 0.0173 | 0.135 | 22,178 |
| C-4 | 7.3 | 0.0161* | 0.130 | 24,924 |
| C-5 | 6.3 | 0.0166* | 0.115 | 20,233 |
| C-6 | 4.5 | 0.0170 | 0.090 | 13,780 |
| C-7 | 4.5 | 0.0168 | 0.085 | 14,110 |
| C-8 | 3.6 | 0.0168 | 0.070 | 11,288 |
| C-9 | 8.5 | 0.0165 | 0.145 | 27,631 |
| C-10 | 10.7 | 0.0165 | 0.160 | 34,782 |
| C-11 | 8.4 | 0.0164 | 0.140 | 27,640 |
| C-12 | 9.5 | 0.0160 | 0.165 | 32,842 |
| C-13 | 8.7 | 0.0159 | 0.143 | 30,456 |
| C-14 | 9.1 | 0.0160 | 0.140 | 31,459 |
| C-15 | 9.3 | 0.0162 | 0.145 | 31,361 |
| C-16 | 8.1 | 0.0159 | 0.140 | 28,355 |
| C-17 | 5.0 | 0.0151 | 0.120 | 19,407 |
| C-18 | 6.0 | 0.0171 | 0.105 | 18,159 |
| C-19 | 5.6 | 0.0177 | 0.110 | 15,819 |
| C-20 | 6.8 | 0.0169 | 0.133 | 21,071 |
| C-21 | 7.6 | 0.0178 | 0.130 | 21,228 |
| C-22 | 4.0 | 0.0170* | 0.080 | 12,249 |
| C-23 | 7.3 | 0.0170 | 0.0135 | 22,355 |
| C-24 | 6.8 | 0.0180 | 0.125 | 18,574 |
| C-25 | 7.5 | 0.0170 | 0.133 | 22,967 |

*Large variation in thickness (over 3 mils from maximum point).

**Table B-17. Results of Completed Cells Lot C Under Four-point Twisting**

| Specimen No. | Fracture Force (lb) | Minimum Thickness (in.) | Relative Deflection at Failure (in.) | Fracture Stress $\tau_s$ (psi) |
|---|---|---|---|---|
| CR-1 | 9.4 | 0.0175 | 0.123 | 27,164 |
| CR-2 | 8.6 | 0.0177 | 0.120 | 24,294 |
| CR-3 | 11.4 | 0.0175 | 0.145 | 32,944 |
| CR-4 | 9.5 | 0.0174 | 0.130 | 27,770 |
| CR-5 | 10.0 | 0.0170 | 0.135 | 30,623 |
| CR-6 | 9.2 | 0.0170 | 0.135 | 28,173 |
| CR-7 | 12.6 | 0.0173 | 0.157 | 37,258 |
| CR-8 | 11.5 | 0.0173 | 0.167 | 34,005 |
| CR-9 | 11.3 | 0.0174 | 0.175 | 33,031 |
| CR-10 | 8.9 | 0.0170 | 0.140 | 27,254 |
| CR-11 | 10.2 | 0.0168 | 0.155 | 31,983 |
| CR-12 | 7.7 | 0.0173 | 0.125 | 22,769 |
| CR-13 | .5 | 0.0177 | 0.065 | 15,537 |

**Table B-18. Results of Completed Cells Lot E Under Four-point Twisting**

| Specimen No. | Fracture Force (lb) | Minimum Thickness (in.) | Relative Deflection at Failure (in.) | Fracture Stress $\tau_s$ (psi) |
|---|---|---|---|---|
| CR-14 | 9.5 | 0.0172 | 0.115 | 28,419 |
| CR-15 | 10.2 | 0.0171 | 0.125 | 30,871 |
| CR-16 | 10.5 | 0.0178 | 0.123 | 29,329 |
| CR-17 | 12.2 | 0.0174 | 0.145 | 35,662 |
| CR-18 | 11.0 | 0.0174 | 0.123 | 32,154 |
| CR-19 | 10.7 | 0.0173 | 0.135 | 31,640 |
| CR-20 | 10.9 | 0.0167 | 0.137 | 34,589 |
| CR-21 | --* | -- | -- | -- |
| CR-22 | --* | -- | -- | -- |
| CR-23 | 7.3 | 0.0176 | 0.103 | 20,856 |
| CR-24 | 9.0 | 0.0171 | 0.125 | 27,239 |
| CR-25 | 12.1 | 0.0170 | 0.178 | 37,054 |
| CR-26 | 7.3 | 0.0180 | 0.125 | 19,940 |
| CR-27 | 10.5 | 0.0177 | 0.145 | 29,6[illegible]1 |
| CR-28 | 14.8 | 0.0177 | 0.195 | 41,808 |

*Sample failed before test.